RUNNING HEAD: Tcf21 in kidney stroma cell fate

The Transcription Factor TCF21 is necessary for adoption of cell fates by Foxd1+ stromal progenitors during kidney development.

Gal Finer[1,2*], Mohammad D. Khan[5], Yalu Zhou[2], Gaurav Gadhvi[5], George S. Yacu[1], Joo-Seop Park[2], R. Ariel Gomez[4], Maria Luisa Sequeira-Lopez[3], Susan E. Quaggin[2,4], and Deborah R. Winter[5].

[1] Division of Pediatric Nephrology, Ann and Robert H. Lurie Children's Hospital of Chicago, Chicago, IL, USA
[2] Feinberg Cardiovascular and Renal Research Institute, Northwestern University Feinberg School of Medicine, Chicago, IL, USA
[3] Department of Pediatrics, Child Health Research Center, University of Virginia, Charlottesville, VA, USA
[4] Division of Nephrology and Hypertension, Northwestern Memorial Hospital, Chicago IL, USA
[5] Division of Rheumatology, Northwestern University Feinberg School of Medicine, Chicago, IL, USA

*Correspondence: *Gal Finer (gal-finer@northwestern.edu), Deborah R. Winter (deborah.winter@northwestern.edu*)

ABSTRACT

Normal kidney development requires coordinated interactions between multiple progenitor cell lineages. The Foxd1+ stromal progenitors are critical for normal nephrogenesis and their heterogeneity is increasingly appreciated. However, the molecular mechanisms and trajectories that drive the differentiation of Foxd1+ cells toward the renal stroma, capsule, mesangial cells, renin cells, pericytes, and vascular smooth muscle cells (VSMCs) are poorly understood. Recent work has implicated Tcf21, a mesoderm-specific bHLH transcription factor critical for embryogenesis, in the development of the kidney stroma and perivascular cells. To investigate the role of Tcf21 in Foxd1+ cells, we performed single-cell RNA sequencing (scRNA-seq) on GFP+ cells from E14.5 *Foxd1*$^{Cre/+}$;*Rosa26*^{mTmG};*Tcf21*$^{f/f}$ kidneys (*Tcf21*-cKO) and controls. Clustering of the entire dataset identified a large stromal population and a smaller representation of non-stromal lineages. Subclustering of stromal cells identified seven populations: medullary/perivascular stroma, proliferating stroma, stroma of the differentiating nephron, nephrogenic zone-associated, collecting duct-associated, and ureteric stroma. Loss of Tcf21 resulted in a dramatic reduction in the medullary/perivascular stroma, proliferating stroma, stroma of the nephrogenic zone, and collecting duct-associated stromal subpopulations. Immunostaining confirmed that *Tcf21*-cKO has a severe constriction of the medullary and collecting duct-associated stromal space. We identified a cluster unique to *Tcf21*-cKO kidneys exhibiting mosaic expression of genes from stromal pogenitors, proliferating, and perivascular cells spanning across all pseudotime, suggesting cells halted in the midst of differentiation. These findings underscore a critical role for Tcf21 in the emergence of Foxd1+ derivatives, with loss of Tcf21 leading to a shift in stromal cell fates that results in abnormal kidney development.

NEW & NOTEWORTHY

The mechanisms responsible for the emergence of renal stromal heterogeneity has been unknown. Using scRNA-seq on Foxd1+ enriched cells from E14.5 kidneys, we identified seven molecularly distinct stromal populations and their regional association. The data suggest that the transcription factor Tcf21 regulates the adoption of fates by Foxd1+ cells that is required to form the normal milieu of stromal derivatives for the development of a kidney of normal size and function.

Keywords: Foxd1; kidney; scRNA-seq; stroma; Tcf21

INTRODUCTION

Work that has spanned over seven decades increased our understanding of molecular mechanisms in kidney development and has been informing new regenerative based solutions for drug screening, disease modelling, and renal replacement (1,2). The developing mammalian kidney is composed of four progenitor lineages: nephron (Six2+ cells), ureteric (Hoxb7+ cells), stromal/interstitial (Foxd1+ cells), and endothelial (c-kit+ cells) (3,4). During kidney development, these progenitor populations signal to each other to ensure the ongoing expansion of the kidney to an organ of normal size and function (5,6). The forkhead box D1 (Foxd1+) progenitors give rise to a diverse array of cell types including most of the renal stroma, vascular smooth muscle cells (VSMCs), pericytes, mesangial cells, renin-, and erythropoietin-producing cells (7,8). Conventionally, renal stroma is divided into three anatomical regions: cortical, medullary, and papillary (9). Recent

research, however, has identified twelve distinct anatomical positions within the stroma in mice, each characterized by unique cell types, highlighting its heterogeneity (10). Foxd1+ cells play critical roles in branching morphogenesis, nephron development, and vascular patterning (11), possibly by promoting maturation of neighboring epithelial and endothelial cells (12-15). Despite these insights, understanding the molecular mechanisms through which the stroma influence non-stromal cells and guide the differentiation of Foxd1+ cells into distinct stromal populations is essential for normal kidney development, yet remains incomplete.

TCF21 is a mesoderm-specific transcription factor of the bHLH family that forms homo/heterodimers upon binding to its target DNA sequence (1,2). Originally named Pod1 (16), epicardin (17), or capsulin (18,19), Tcf21 is expressed in the developing urogenital, cardiovascular, respiratory, and gastrointestinal systems during embryonic development. Tcf21 has been recently implicated as a causal gene for coronary artery disease in humans (20,21). Within the kidney, Tcf21 has been implicated in the formation of the renal stroma and perivascular cells, influencing the structural integrity and function of the organ (22). To investigate the role of Tcf21 on the development of kidney stroma, we performed scRNA-seq on normal and Tcf21-deficient Foxd1+ kidney cells from E14.5 mouse embryos, an early stage of nephrogenesis.

MATERIALS AND METHODS

Mouse strains and embryo staging

All mouse experiments were approved by the Animal Care Committee at the Center for Comparative Medicine of Northwestern University (Evanston, IL) and were performed in accordance with institutional guidelines and the NIH Guide for the Care and Use of Laboratory(6) Animals. For gestational age, noon of the day on which the mating plug was observed was designated E0.5. Sex was determined before analysis and samples were pooled accordingly. The following mice were used in the studies described: *Tcf21*$^{floxf/lox}$ was created as previously described (23), *Foxd1-eGFPCre* (JAX Stock #012463), Rosa26Tomato (JAX Stock #007909). Genotyping was performed with Quick-Load Taq 2X Master Mix (M0271L, BioLabs) on 2% agarose gel for the PCR bands.

Histology and immunohistochemistry

Mouse embryo dissections were performed at the indicated time-points. Samples were fixed with 10% Neutral buffered formalin or 4% paraformaldehyde overnight, embedded in paraffin, and sectioned into 5µm by the Mouse Histology and Phenotyping Laboratory of Northwestern University. Sections were deparaffinized in xylene and ethanol and boiled in citrate buffer for antigen retrieval. Sections were then treated with 1% donkey serum with 0.3% TritonX100 in PBS for 30 minutes at room temperature before incubating with primary antibodies at 4°C overnight. Sections were washed in PBS and incubated with anti-GFP antibody (A11122, Life Tchnologies, 1:1000). Alexa Fluor 488 fluorescence-conjugated secondary antibody was incubated for 45 minutes at room temperature.

Preparation of single cells from E14.5 mouse embryos

E14.5 *Foxd1*^{Cre}*;Rosa26*^{mTmG}*;Tcf21*$^{f/f}$ and *Foxd1*^{Cre}*;Rosa26*^{mTmG}*;Tcf21*$^{+/+}$ mouse embryos were excised and kidneys were dissected and washed in cold PBS without calcium or magnesium. Cell dissociation was performed as previously described (24). Briefly, the kidneys were minced and digested with freshly prepared mix of Collagenase type 2 (Worthington, LS004174, 2.5mg/ml), DNase I (Worthington, LS002058, 125u/ml), and Licheniformis Protease 7.5mg/ml by incubating for 40 min at 6 deg Celsius with manual dissociation via pipetting every 5 minutes. Digestion was inactivated using stop solution of 20% FBS in PBS (Ca-, Mg-). After pelleting the cells at 1250 rpm for 7 min, cells were resuspended in 1 ml of DMEM (Dulbecco's Modified Eagle Medium, Gibco, Netherlands) + FBS 2% and passed through a 40uM" strainer (Scienceware Flowmi, H13680-0040) into DNA LoBind tubes (Eppendorf, 022431005)). Cells were resuspended in 500 µl DMEM + FBS 2% and filtered two more times through to a 5 ml polypropylene round bottom tube (Falcon™ 352063). Cells were sorted at the Flow Cytometry Cell Sorting core at Northwestern University on a BD FACSAria SORP system and the BD FACSymphony S6 SORP system. GFP positive cells were collected and resuspended in PBS with 1%BSA (Bovine Serum Albumin) for immediate use. Samples of shared sex and genotyping were pooled leading to 4 samples.

Initial Processing of Single-cell RNA-seq

Single cells were processed using the 10x Genomics Chromium 3' Kit version 3 and sequenced on an Illumina NovaSeq with a target of ~400,000,000 reads per sample. Raw sequencing data was demultiplexed and processed using Cell Ranger v6.1.0 and a custom reference combining the mm10 transcriptome with the eGFP and tdTomato RNA sequences. Filtered count metrics from each sample were loaded as a Seurat object (v4.0.2). Genes were retained in the analysis only if expressed in at least three cells. Cells exhibiting fewer than 2000 or more than 8000 gene features were filtered out of the subsequent analysis. Moreover, cells with mitochondrial content exceeding 15% or with hemoglobin gene (Hba and Hbb) expression above 1%, were also discarded. Following this, Scrublet (v0.2.2) was used to identify cells likely to be doublets, applying

25 principal components for each sample. Across all samples, an expected doublet rate threshold of 7.6% (based on loading of approximately 16,000 cells) was set to ensure thorough and consistent doublet identification leading to 2701 cells marked for removal. After filtering, all samples were merged into a single Seurat object. Estimated cells numbers and initial quality control (QC) statistics are given in the table below:

Sample	Pre-QC Cell #	Median Genes	Median UMIs	% Reads in Cell	Post-QC Cell #
Control Female	11,049	3,570	12,569	95.5	9526
Control Male	11,995	3,946	15,391	94.7	9679
Mutant Female	7,867	4,468	18,576	93.2	5830
Mutant Male	9,543	4,387	19,294	94.0	7426
Total					**32,461**

Cell Type Annotation

SCTransform was applied on 3000 variable genes for data normalization and scaling, with UMI count and percent mitochondria set as variables to regress. Principal component analysis (runPCA) was performed across all samples and the first 25 PCs were selected for Uniform Manifold Approximation and Projection (UMAP). Clustering (FindClusters) was also run with 25 PCs and a resolution parameter of 0.25. To identify *de novo* markers for the resulting 13 clusters, FindMarkers was run using a two-sided Wilcoxon rank-sum test (min. pct = 0.25) with adjusted p-value calculated using Benjamini-Hochberg method. Individual clusters were grouped together based on annotated cell type for further analysis.

Stromal Subclustering

To identify sub-populations within stromal clusters, we selected all cells from the clusters annotated as stroma (n = 22,355). Cells exhibiting more than 10% mitochondrial content were excluded to eliminate stressed or dying cells that could skew the analysis.

Sample	All Stromal Cells	Median Genes	Median UMIs	Filtered Stromal Cells
Control Female	8912	3577	12558	8897
Control Male	6724	3889	14559	6689
Mutant Female	4939	4668	19993	4934
Mutant Male	1780	4046	14959	1777
Total	**22,355**	**3922**	**14,644**	**22,297**

The remaining 22,297 cells were renormalized using scTransform with 3000 variable genes and regressing on the difference between S and G2M score (CellCycleScoring) as recommended by Seurat to limit the effect of cell cycle on clustering while maintaining differentiation-associated trends. UMAP and clustering (FindClusters) were performed with the first 15 principal components and resolution at 0.20. *De* novo markers across stromal clusters were identified as described above for cell types. Transcriptional signatures of stromal compartments were calculated using AddModuleScore on curated markers based on publicly available sources (10,25), Allen Developing Mouse Brain Atlas (https://developingmouse.brain-map.org/), GUDMAP (26,27), and our previous studies (22) (**Suppl Fig. S3**). To compare our annotations to previously published clusters (Combes et al), we calculated the fraction of the top 20 published markers that overlapped our list of *de novo* markers by cluster.

GenePaint

The spatial expression of representative key genes in control E14.5 mouse kidney was examined using *GenePaint* gene expression atlas (https://gp3.mpg.de/).

Comparison of Stromal Cells in *Tcf21*-cKO and Control

Before comparing stromal cells across genotype, each sample was subsampled to 1777 stromal cells to match the lowest sample and ensure even numbers across sexes. The scProportionTest algorithm

(https://github.com/rpolicastro/scProportionTest) was used to calculate p-values for differences in composition between *Tcf21*-cKO and control conditions using a permutation test. Confidence intervals were provided through bootstrapping. Differential expression analysis between conditions was performed using FindMarkers on all stromal cells in *Tcf21*-cKO vs. control (min.pct = 0.25). Genes with log fold change ≥ 0.25 and with p-adjusted value less than ≤ 0.05 were defined as significantly increased or decreased in expression. Enriched GO terms for genes that exhibited significantly increased or decreased expression in *Tcf21*-cKO were determined using the R package clusterProfiler (https://github.com/YuLab-SMU/clusterProfiler) and compared all 28,891 genes expressed in the dataset as background.

Trajectory Analysis

To construct a pseudotime trajectory representing healthy differentiation, cells from control samples (n = 15,579, excluding 7 outlier cells from the ECM-expressing cluster) were isolated from the stromal population. This subset of cells was normalized using scTransform with regression by cell cycle score difference as above (S-G2M). Then, RunPCA and RunUMAP (dim=15) was performed. The two-dimensional representations was converted to be compatible with Monocle v3 (28,29). Clustering was performed in Monocle using the cluster_cells function with default parameters. To build the underlying trajectory, learn_graph was run with parameters close_loop=FALSE and ncenter=310 (chosen based on calculating 2% of the number of cells). The starting node was chosen to reflect the Nephogenic zone stroma using order_cells(). All the trajectory graphs were visualized using the plot_cells() function with or without a trajectory graph. The function graph_test() was used to identify co-regulated genes across pseudotime with the autocorrelation approach ("principal_graph" parameter). Significant genes were defined by q value < 0.05. Genes were grouped into modules using find_gene_modules() with default parameters testing a range of resolution values from 10^{-6} to 10^{-1} and the aggregate_gene_expression was used to calculate module expression. To quantify changes in module expression between *Tcf21*-cKO and control clusters, the number of cells with score greater than 0 was calculated as a percent of total cell in cluster.

RESULTS

Single-cell profiling of E14.5 *Foxd1* GFP+ cells identifies diverse cell populations within the developing kidney

To investigate the role of Tcf21 in the Foxd1+ stromal progenitors and their derivative cells at a single-cell level, we purified GFP+ cells from male and female *Foxd1*$^{Cre/+}$;*Rosa26*^{mTmG};*Tcf21*$^{f/f}$ (*Tcf21*-cKO) and littermate controls *Foxd1*$^{Cre/+}$;*Rosa26*^{mTmG};*Tcf21*$^{+/+}$ via flow cytometry. In this model, *Tcf21* gene is permanently deleted, tdTomato expression is terminated, and GFP expression is maintained in all the progeny of Foxd1-expressing cells. We obtained 13,256 cKO and 19,205 control cells after QC (**Suppl Fig. S1a**). We defined 13 clusters using an unsupervised approach (see Methods) and assigned cell lineage annotations based on *de novo* markers and canonical gene expression (**Fig.1a-b, Suppl Fig. S1c-d**). This analysis identified a large population of stromal cells (Foxd1+ Meis1+ Pdgfra+) as well as representation of the nephron progenitor cell (NPC) lineage (Six2, Cited1, Crym), and significantly smaller populations of ureteric epithelium (Ret, Wnt 11, Gata3), immune cells (Fcer1g, Lyz2), and neurons cells (Tubb3, Map2) (**Fig.1a-b, Suppl Fig. S1d-e**). Cycling genes were expressed across cell lineages (**Suppl Fig. S1f**). We confirmed that GFP expression was robust in both stromal and non-stromal cells, though Foxd1 expression was largely limited to the stromal lineage (**Fig. 1c**). Low expression of tdTomato and depleted expression of Tcf21 in *Tcf21*-cKO cells validate the activity of cre recombinase in these cells (**Fig. 1c, Suppl Fig. S1g**). Non-stromal GFP+ cells likely represent early transient expression of Foxd1 before the onset of lineage boundaries. Expression of Foxd1 in NPC has been reported by others (8,30-33) and is thought to stem from a shared signature during early nephrogenesis (25). Additionally, autofluorescence generated by non-stromal cell types may have overlapped with the GFP channel. Tcf21 expression was detected in the stromal and NPC lineages, consistent with previous reports (34) (**Fig. 1c, Suppl Fig. S1g**). All cell types were represented in both males and females of *Tcf21*-cKO and control samples, however the proportion of stromal cells was lower in mutant samples (**Fig. 1d**, **Suppl Fig. S1h**).

E14.5 stromal progenitors express genes associated with different cell fates

Next, we sought to explore the heterogeneity within the developing stromal cell populations by sub-clustering cells annotated as stroma (**Suppl Fig. S2a-b**). We defined seven stromal subpopulations (numbered 0-6) in both *Tcf21*-cKO and controls with distinct gene expression profiles based on *de novo* marker expression (**Fig. 2a-b**). All clusters expressed similar levels of GFP and low level expression of tdTomato although expression of *Foxd1* and *Tcf21* was variable (**Suppl Fig. S2c**). To annotate these clusters, we created modules of stromal cell markers from the literature (**Suppl Fig. S3**) and visualized their expression along with canonical cell cycles genes (**Fig. 2c**). We annotated Nephrogenic zone associated stroma based on high expression of genes localized to the cortical/Nephrogenic zone of the kidney (*Foxd1, Crabp2, Gdnf, Aldh1a2, Ntn1, Igfbp5, Plag1, Fibin);* Proliferating stromal cells based on strong cell cycle signature (*Rrm2, Pclaf, Lig1*); Medullary/Perivascular associated stroma based on combined expression of gene localized to the kidney medulla (*Clca3a,*

Ace2 , Igfbp3, Acta2, Col4a1, Zeb2, Col1a1, and Tgfb1i1) and genes expressed in perivascular cells *(Rgs5, Heyl2, Akr1b7, Ren1, Pdgfrb, Mef2c, Angpt2)*; Collecting duct associated stroma based on *Penk, Pfn2, Tcf21, Thy1, Lef1, Alx1, Sema3c, Wnt4*; stroma of the Differentiating nephron uniquely expressed *Smoc2, Igf1, Dcn, Fbln5*; and Ureteric stroma based on *Tbx18, Syt1, Np71r, and Dlk1*. To confirm our annotations, we compared expression of key genes in our single-cell data vs. spatial expression from the *GenePaint* gene expression atlas (**Fig. 3**). Our annotations largely agreed with previously published stromal clusters during kidney development (Combes et al (25)), except for one instance (**Suppl Fig. S2d-e**). Our annotated Differentiating nephron cluster (cluster 3) resembles the published Ureteric cluster. However, the low levels of *Tbx18* in cluster 3 did not support its classification as Ureteric. Tbx18 is known to play a critical role in the early separation of the ureteric mesenchymal lineage from other mesenchymal lineages (11) (35). Additionally, we annotated cluster 2 as Emcn-expressing based on unique expression of the gene Endomucin (*Emcn*), further discussed in the following section (**Fig. 2, Fig. S2f**).

Tcf21 is required for emergence of stromal sub-populations during kidney development

Next, we sought to determine how stromal progenitor cells in *Tcf21*-cKO have deviated from controls. Strikingly, Nephrogenic zone, Proliferating, Medullary/Perivascular, and Collecting duct associated stroma clusters were dramatically reduced in *Tcf21*-cKO compared to control (**Fig. 4a-c**). Conversely, Ureteric-associated stroma and Differentiating nephron-associated stroma clusters showed moderately increase in *Tcf21*-cKO. Notably, the most profound change was that the Emcn-expressing cluster was virtually exclusive to *Tcf21*-cKO kidneys, with only few cells (7 cells) of shared transcriptional profile identified in stromal cells of controls (**Fig. 4a-c**). This population exhibits high levels of *Rgs5* (indicative of VSMC fate) and and *Sparcl1* of the extracellular matrix (**Suppl Fig 4a).**

In parallel, we performed differential gene expression analysis of the whole stromal compartment between *Tcf21*-cKO and control (**Suppl Table S3b**). We identified 214 genes up-regulated and 113 genes down-regulated in *Tcf21*-cKO compared with control cells (**Fig. 4d**). Tcf21 is among the most down-regulated genes, as expected, while genes associated with connective tissue development, epithelial cell proliferation, and WNT pathway were upregulated (**Fig. 4e**). In order to determine how the Emcn-expressing cells fit into healthy stromal cell differentiation, we ran Monocle on control stromal cells to estimate the underlying pseudotime trajectory. By transferring control-based pseudotime to *Tcf21*-cKO cells, we found that the Emcn-expressing cluster comprised cells spanning across all pseudotime (**Fig. 4f-g**). Moreover, when we defined co-regulated modules genes along the trajectory, we found that cell subsets of the Emcn-expressing cluster expressed gene clusters including nephrogenic (module 18), proliferating (module 20), and medullary/perivascular (module 14) (**Suppl Fig. 4c-d**). Taken together, these results suggest that the *Tcf21*-cKO is associated with an increase in cells that are halted in the midst of differentiation.

To spatially define the defect in the stromal lineage of the *Tcf21*-cKO, we performed lineage-tracing of Foxd1 (GFP+) in *Foxd1*$^{Cre/+}$*;Rosa26*^{mTmG}*;Tcf21*$^{f/f}$ and control mice from E14.5 to E18.5. *Tcf21*-cKO demonstrated a marked constriction of the medullary stroma and the stromal space adjacent to the collecting ducts compared with controls (**Fig. 5a**). Additionally, immunostaining for endomucin, a marker of the stromal population exclusively expressed in *Tcf21* cKO, confirmed robust expression of endomucin solely in the stromal lineage of *Tcf21*-cKO kidneys at E14.5 and E16.5 (**Fig. 5b**). Furthermore, staining with alpha smooth muscle actin (Acta2), which marks medullary stromal cells ((10) and (22)), demonstrated a loss of Acta2-expressing stroma and the emergence of Emcn-positive stromal cells in *Tcf21*-cKO kidneys (**Fig. 5c**), supporting a population shift. Taken together, these data support the scRNA-seq analysis results above and indicate a requirement for Tcf21 in the emergence of specific derivatives of the stromal lineage during kidney development.

DISCUSSION

Our findings underscore the critical role of Tcf21 in the differentiation and fate determination of Foxd1+ stromal progenitors during kidney development. Using scRNA-seq and detailed sub-clustering analysis, we identified seven distinct stromal populations within the developing kidney. The deletion of Tcf21 led to a significant reduction in specific stromal populations, including medullary/perivascular stroma, proliferating stroma, nephrogenic zone-associated stroma, and collecting duct-associated stroma. Concurrently, a novel stromal population emerged in Tcf21-deficient kidneys, characterized by high expression of Endomucin, a gene from the sialomucin family typically expressed in endothelial cells of the vasculature. This new population was annotated as Endomucin-expressing stroma. Our trajectory analysis indicated that this novel stromal population represents cells arrested in their differentiation process.

The kidney stromal compartment is known for its high heterogeneity, with Foxd1+ progenitors giving rise to diverse cell types such as fibroblasts, VSMCs, pericytes, renin cells, and mesangial cells. Previous studies have highlighted the pivotal roles of Foxd1+ cells in branching morphogenesis, nephron development, and vascular patterning. However, until now, the molecular mechanisms guiding the differentiation of these cells into distinct stromal lineages have been poorly understood. The medullary and collecting duct stromal compartments are particularly crucial for the kidney's structural integrity and function. The medullary stroma/interstitium is essential for maintaining the osmotic gradient required for urine

concentration, while the collecting duct-associated stroma plays a vital role in the development and function of the collecting duct. The loss of these stromal populations in *Tcf21*-cKO was associated with disrupted collecting duct organization and a urine concentrated defect after birth (22). Mechanistically, Tcf21 may facilitate Foxd1+ cell proliferation at E14.5, which aligns with our observations at E16.5 and E18.5, as well as with reports of Tcf21's inhibition of cell cycle arrest-promoting factors (36).

The identification of a distinct stromal population exclusively present in Tcf21-depleted Foxd1+ cells, characterized by unique expression of endomucin, and by upregulation of genes marking vascular smooth muscle cell fate (*Rgs5*) and extracellular matrix components (*Sparcl1*), suggests that Tcf21 may play a critical role in VSMC formation during kidney development. Our trajectory analysis indicates that this novel stromal population represents cells arrested in their differentiation process, drawing parallels to Tcf21's known role in VSMC phenotypic modulation in human coronary artery disease (37). Histological analysis identified the novel Endomucin-expressing stroma in *Tcf21-cKO*, which was associated with a concurrent decrease in medullary Acta2-expressing stromal cells, supporting a population shift. This aspect of Tcf21 function may shed light on how Tcf21 influences VSMC differentiation and vascular integrity, consistent with our previous finding of disrupted arterial tree in *Foxd1Cre;Tcf21 cKO* (22).

Interestingly, we observed an increase in ureteric-associated stroma and differentiating nephron-associated stroma in *Tcf21-cKO* kidneys, suggesting potential compensatory mechanisms or shifts in cell fate in response to Tcf21 loss. Lineage tracing for Foxd1 revealed a global reduction in the stromal space at E14.5, while the medullary stroma was predominantly affected at E16.5 and E18.5, consistent with compensation. High Tcf21 expression in proliferating, medullary/perivascular, and collecting duct-associated stroma, compared to nephrogenic zone cells, suggests that Tcf21 action occurs upon Foxd1+ cell priming. Conversely, low Tcf21 expression in ureteric stromal clusters and the independence of these populations from Tcf21 indicate that the emergence of stromal cells surrounding the ureter is not dependent on Tcf21 expression in Foxd1+ cells.

Gene Ontology enrichment analysis between *Tcf21-cKO* and control stromal cells revealed significant changes in genes involved in connective tissue development, epithelial cell proliferation, and WNT signaling pathways. The downregulation of *Tcf21* itself in *Tcf21*-cKO cells further validates the effectiveness of our genetic model.

Our data proposes a model in which Tcf21 plays a critical role in the differentiation of Foxd1+ stromal progenitors during kidney development by regulating the emergence and composition of distinct stromal populations, thereby ensuring proper kidney development and function (**Fig. 5d**).

Beyond kidney development, our findings suggest broader implications for Tcf21 in mesodermal development, including the heart and respiratory systems, expanding our understanding of Tcf21's role in these tissues and its potential impact on fibrotic diseases characterized by excessive ECM deposition. This study is limited by a single time point of scRNA-seq, which restricts cell annotation and interpretation of definitive cell fates. Further studies are required to identify transcriptional networks, direct targets, and signaling pathways in Tcf21 regulatory networks in the regulatory of Tcf21 in Foxd1+ cells.

DATA AVAILABILITY

Data will be uploaded to the Gene Expression Omnibus upon acceptance of the manuscript.

SUPPLEMENTAL MATERIAL

Supplemental Figs. S1–S3:
Suppl Fig. S1: QC panels and UMAP of original de novo clustering and heat map of top markers
Suppl Fig. S2: QC of scRNA-seq analysis of stromal cells
Suppl Fig. S3: Stromal cell-type markers for module scores
Suppl Fig. S4: Monocle modules

Supplemental Tables S1–S5:
Suppl Table S1: a. All cluster markers. b. Cell type markers
Suppl Table S2: a. Stromal subclustering markers. b. Marker overlap with Combes et al
Suppl Table S3: a. Downsampled cell numbers by stromal cluster by sample b. Differential gene expression output c.Go term output
Supp Table S4. Monocle module genes

ACKNOWLEDGMENTS

This work was supported by the Northwestern University Robert H Lurie Comprehensive Cancer Center Core Facilities, including Flow Cytometry Core, Mouse Histology and Phenotyping Laboratory (MHPL) and NUSeq Core. Microscopy was provided by the Center for Advanced Microscopy of Northwetsern University and by the Microscopy and Histology

Group at Stanley Manne Children's Research Institute affiliated with Ann and Robert H. Lurie Children's Hospital of Chicago.
We thank Dr. Matthew Schipma and Ms. Wai at NUSeq, Mr. Mehl at flow cytometry, Ms. Acar at MHPL for technical supports. We also thank Dr. Benjamin Thomson and other members of the Quaggin lab for helpful discussions.
This research was supported in part through the computational resources and staff contributions provided by the Genomics Compute Cluster which is jointly supported by the Feinberg School of Medicine, the Center for Genetic Medicine, and Feinberg's Department of Biochemistry and Molecular Genetics, the Office of the Provost, the Office for Research, and Northwestern Information Technology. The Genomics Compute Cluster is part of Quest, Northwestern University's high performance computing facility, with the purpose to advance research in genomics.
With gratitude to the Zell Family Foundation.

GRANTS

National Institute of Health, US Department of Human Health and Services, 1K08 DK118180-01A1 (to Gal Finer). The Winter Lab is supported by the American Heart Association (AHA: 18CDA34110224), the American Thoracic Society (ATS), and the NIH (R01 AI163742; R01AR080513; R21AR080351; R01AR075423).

DISCLOSURES

Susan E. Quaggin holds patents related to therapeutic targeting of the ANGPT-TEK pathway in ocular hypertension and glaucoma and owns stock in and is a director of Mannin Research. S. Quaggin also receives consulting fees from AstraZeneca, Janssen, the Lowy Medical Research Foundation, Roche/Genentech, Novartis, and Pfizer and is a scientific advisor or member of AstraZeneca, Genentech/Roche, JCI, the Karolinska CVRM Institute, the Lowy Medical Research Institute, Mannin, Novartis and Goldilocks. DRW received consulting fees from Pfizer during the duration of this project. All other authors have nothing to disclose.

FIGURE LEGENDS

Figure 1: scRNA-seq analysis of the entire Foxd1GFP+ sorted cells from E14.5 embryonic mouse kidneys of *Tcf21*-cKO and controls. (a) UMAP plot of 32,461 cells combined from control and *Tcf21*-cKO samples projected in two dimensions. Each dot represents a single cell, and each color denotes a cell-type annotation. Six clusters of Foxd1GFP+ cells from E14.5 developing mouse kidneys were identified. Each cluster represents a distinct cell lineage based on the expression of the following canonical markers: stromal cell identity (*Foxd1, Meis1, Pdgfra*), nephron progenitor cell (NPC) identity (*Six2, Cited1, Crym*), ureteric epithelium identity (*Ret, Wnt 11, Gata3*), endothelial identity (*Pecam1, Cd34*), immune cell identity (*Fcer1g, Lyz2*), and Neuron identity (*Tubb3, Map2*). (b) DotPlot illustrating key cell-type markers across the Foxd1GFP+ cell clusters. Each dot represents gene expression within the indicating cell type, with the color representing relative expression level, and the dot size indicating the percentage of cells that expressed the gene within each cell type. Note the low expression of stromal markers in non-stromal clusters of kidney cells, except for NPC cluster, which expresses low levels of *Foxd1* and *Meis1*. (c) UMAP plots of normalized EGFP, Foxd1, tdTomato, and Tcf21 gene expression. EGFP expression is shown in the entire dataset of FACS sorted cells. Foxd1 expression in the entire dataset demonstrates high levels in stromal cells compared to other lineages. Low expression of tdTomato and depleted expression of Tcf21 in *Tcf21*-cKO cells validate the activity of cre recombinase in these cells. Scale represents normalized log2-expression. (d) UMAP plot of samples by experimental group and sex. All cell types are represented in kidneys from females and males of controls and *Tcf21*-cKO. The stromal population is smaller in kidneys from *Tcf21*-cKO, with higher representation of non-stromal lineages. (n=1 independent experiment using cells pooled from n=4 control males, n=2 control females, n=1 cKO male, n=3 cKO females. See **Suppl Fig. S1** for number of cells per experimental group.

Figure 2: Stromal lineage sub-clustering identifies populations of distinct cell fate within the developing mouse kidney. (a) Sub-clustering of stromal cells (n=22,297) from E14.5 Foxd1GFP+ kidney cells (stromal cluster in **Fig. 1a**) identifies seven transcriptionally distinct populations and their suggested annotation. (b) Single-cell heat map depicting the expression of the top 5 cluster markers, with genes shown on the right. Column color coding is consistent with **Fig. 2a.** Yellow indicates high expression of a particular gene, and purple indicates low expression. (c) Module score distribution in UMAP space for the eight cell-type gene signatures evaluated (listed in **Suppl Fig. 3**) using Seurat's AddModuleScore.

Figure 3: Spatial annotation of stromal clusters of control and *Tcf21*-cKO. (a) Feature plots showing the Log-normalized expression of markers for Nephrogenic zone stroma (*Foxd1, Crabp2, Gdnf, Aldh1a2*), Medullary and Perivascular stroma (*Pdgfrb, Ace2, Rgs5, Heyl*), Collecting duct stroma (*Penk, Pfn2, Tcf21, Thy1)*, stroma of the Differentiating nephron (*Smoc2, Igf1, Dcn, Fbln5*), and Ureteric stroma (*Tbx18, Syt1, Npy1r)*. (b) Expression of key marker genes of each cluster spatially represented by in-situ hybridization in control E14 mouse kidneys as per *GenePaint* gene

expression atlas (https://gp3.mpg.de/, cropped images from whole mount). (c) Schematic illustration of the spatial location of each stromal population in the developing kidney. Cluster 0 (Medullary and Perivascular stroma), cluster 4 (Nephrogenic zone stroma), cluster 5 (Collecting duct stroma), cluster 3 (stroma of the Differentiating nephron), and cluster 6 (Ureteric stroma).

Figure 4: Tcf21 is critical for the development of specific stromal cell fates. (a) UMAPs of Foxd1GFP+ stromal cells from E14.5 control and *Tcf21*-cKO mouse kidneys ($Foxd1^{Cre/+};Rosa26^{mTmG};Tcf21^{+/+}$ and $Foxd1^{Cre/+};Rosa26^{mTmG};Tcf21^{f/f}$, respectively). All stromal subpopulations that were identified in control kidneys are present in cKO but with a dramatic reduction in clusters 0, 1, 4, and 5, corresponding to Proliferating, Medullary/Perivascular, Nephrogenic zone, and Collecting ducts associated stroma, as is indicated by the proportion test. (b) Cell-type composition stacked bar chart by sample. Cell counts for each sample are normalized to 100%. (c) Relative differences in cell proportions for each cluster between the *Tcf21*-cKO versus control. Dashed vertical lines mark FDR < 0.05 and mean | Log_2 fold enrichment | > 1 compared with the control (permutation test; n = 7,108). (d) Differentially expressed genes (DEGs) were determined by log_2(fold change >0.25 and adjusted p-value <0.05. Red and blue dots denote significantly up- and down-regulated differential genes, respectively. 214 genes were up-regulated and 64 genes were down-regulated in cKO vs. control cells. (e) GO Terms of differentially expressed genes, up-regulated (top panel) and down-regulated (bottom panel), as a scatter diagram with a degree of enrichment by the richness factor (number of overlap genes/ Gene in process), p-adjust, and the number of genes enriched in a pathway. The number of enriched DEGs in the pathway is indicated by the circle area, and the circle colour represents the ranges of the p-adjust. (f) UMAP plot of stromal sub-clusters, with color-coding based on pseudobins generated from Monocle3 pseudotime binning. (g) Whiskers box plot depicting the range of pseudobins across each stromal sub-clusters.

Figure 5: Lineage Tracing and Population Shift in Foxd1+ Stromal Cells of *Tcf21*-cKO Kidneys. (a) Lineage tracing for Foxd1+ cells. Immunofluorescence (IF) staining of $Foxd1^{Cre/+};Rosa26^{mTmG};Tcf21^{f/f}$ and control kidneys using an anti-GFP antibody shows a significant reduction in the stromal space in *Tcf21*-cKO at E14.5, consistent with scRNA-seq findings. Lineage tracing at E15.5, E16.5, and E18.5 indicates that the loss of stromal space persists in medullary stroma and stroma adjacent to the collecting ducts in *Tcf21*-cKO kidneys (dotted line). Scale bar 500 µm. **(b-c) Histological validation of scRNA-seq population shift.** (b) IF staining reveals the presence of the novel Endomucin-positive stromal cells (arrowheads in bottom panel) in *Tcf21*-cKO at E14.5 and E16.5. In contrast, Endomucin expression is restricted to the endothelium and absent in stromal cells in control kidneys (arrow in top panel). (c) Loss of alpha smooth muscle beta-actin (Acta2)-positive stromal cells (arrowheads in top panel) in *Tcf21*-cKO at E16.5 and E18.5. This loss coincides with the appearance of Endomucin-positive stromal cells (arrowheads in bottom panel), supporting the hypothesis of a population shift. **(d) Schematic illustration of major findings.** (left) Anatomical mapping of main kidney progenitor lineages, including stroma, endothelial, ureteric bud, and nephron progenitors, identified in initial scRNA-seq clustering. (right) Anatomical mapping of stromal cell subpopulations identified in scRNA-seq stromal subclustering. Control samples showed six stromal populations (nephrogenic zone-associated, proliferating, medullary/perivascular, collecting duct-associated, differentiating nephron-associated, and ureteric stroma). In contrast, *Tcf21*-cKO samples exhibited a loss of nephrogenic zone-associated, proliferating, medullary/perivascular, collecting duct-associated stroma, along with the emergence of a novel Endomucin-expressing stromal cell population.

Supplemental Figure S1: Quality control of scRNA-seq analysis of entire Foxd1GFP+ sorted cells from control and *Tcf21*-cKO kidneys. (a) Violin plots illustrating number of genes, unique molecular identifiers (UMIs), and percentage of mitochondrial genes from control and *Tcf21*-cKO E14.5 kidney samples. (b) Uniform manifold approximation and projection (UMAP) plot showing the singlets and doublets assignment in control and *Tcf21*-cKO mice. (c) Single-cell heat map depicting the expression of the top 5 markers per cluster with genes shown on the right. Column color coding is consistent with **Suppl Fig. 1d.** (d) UMAP plot showing the unbiased classification of cells from control and *Tcf21*-cKO mice. Thirteen clusters were defined and annotated as stromal (clusters 0,1,2,5,6,7), nephron progenitor cells (NPC) (clusters 3,4,8), epithelial (cluster 9), endothelial (cluster 11), immune (cluster 10), or neuron (cluster 12). (e) Violin plots showing gene expression of the stromal markers *Pdgfra* and *Meis1* across clusters. The *y*-axis shows normalized expression level as probability distribution across clusters. (f) UMAP embedding of cells from control and *Tcf21*-cKO kidneys colored by cell-cycle position estimated using CellCycleScoring. (g) Violin plots illustrating normalized Tcf21 gene expression across clusters for control (blue) and *Tcf21*-cKO (red) samples. (h) Stacked bar plot displaying number of cells for main cell type separated by experimental group and sex.

Supplemental Figure S2: Quality control of scRNA-seq analysis of stromal cells. (a) Violin plots illustrating number of genes, unique molecular identifiers (UMIs), and percentage of mitochondrial genes of control and *Tcf21*-cKO stromal sub-

clusters. (b) UMAP plot showing the stromal subpopulations embedded onto the merged control and *Tcf21*-cKO mice data. (c) Violin plots illustrating normalized EGFP, Foxd1, tdTomato, and Tcf21 gene expression across stromal subpopulations for control (blue) and *Tcf21*-cKO (red) samples. (d) Heatmap depicting the expression of stromal cell-type markers (left) and cluster annotation (right) as per Combes et al. (25) across our stromal subpopulations. Color scale represents log-fold change in differential expression. (e) Heatmap depicting scaled values for the number of overlapped genes. Columns represent control and *Tcf21*-cKO stromal populations, while rows represent stromal cluster annotation as per Combes et al (25). (f) Feature plot showing the log normalized expression of Endomucin. (g) Violin plots illustrating Endomucin gene expression across clusters for control (blue) and *Tcf21*-cKO (red) samples.

Supplemental Figure S3: Stromal cell-type markers for module scores. Listing of the six distinct cell types, their respective gene sets, and references from which these genes were sourced, which were used to calculate module scores for **Fig. 2c**.

Supplemental Figure S4: (a) Violin plots illustrating the normalized expression of up-regulated genes (Tgfb2, Sparcl1, Postn, and Rgs5) across stromal subpopulations, for control (blue) and *Tcf21*-cKO (red) samples. (b) Violin plots illustrating the normalized expression of down-regulated genes (Snai2, Ifitm1, Dkk1, Acta2) across stromal subpopulations, for control (blue) and *Tcf21*-cKO (red) samples. (c) Heatmap displaying the relative expression of module scores across each stromal subpopulation. Rows correspond to module set numbers, while column annotations at the bottom indicate stromal populations. (d) Feature plots showing module scores for gene sets from module18, module20, and module14, calculated using the AddModuleScore() function across each stromal subpopulation. Genotypes are distinguished by color (blue for control, red for *Tcf21*-cKO).

1. Lawlor KT, Vanslambrouck JM, Higgins JW, Chambon A, Bishard K, Arndt D, Er PX, Wilson SB, Howden SE, Tan KS, Li F, Hale LJ, Shepherd B, Pentoney S, Presnell SC, Chen AE, Little MH. Cellular extrusion bioprinting improves kidney organoid reproducibility and conformation. *Nat Mater*. Feb 2021;20(2):260-271. doi:10.1038/s41563-020-00853-9, PMCID: PMC7855371.
2. Dorison A, Forbes TA, Little MH. What can we learn from kidney organoids? *Kidney Int*. Nov 2022;102(5):1013-1029. doi:10.1016/j.kint.2022.06.032, PMID: 35970244.
3. Walker KA, Bertram JF. Kidney development: core curriculum 2011. *Am J Kidney Dis*. Jun 2011;57(6):948-958. doi:10.1053/j.ajkd.2011.03.009, PMID: 21514985.
4. Merlet-Benichou C. Influence of fetal environment on kidney development. *Int J Dev Biol*. 1999;43(5):453-456. PMID: 10535323.
5. Little MH, McMahon AP. Mammalian kidney development: principles, progress, and projections. *Cold Spring Harb Perspect Biol*. May 1 2012;4(5)doi:10.1101/cshperspect.a008300, PMCID: PMC3331696.
6. McMahon AP. Development of the Mammalian Kidney. *Curr Top Dev Biol*. 2016;117:31-64. doi:10.1016/bs.ctdb.2015.10.010, PMCID: PMC5007134.
7. Sequeira-Lopez ML, Lin EE, Li M, Hu Y, Sigmund CD, Gomez RA. The earliest metanephric arteriolar progenitors and their role in kidney vascular development. *Am J Physiol Regul Integr Comp Physiol*. Jan 15 2015;308(2):R138-149. doi:10.1152/ajpregu.00428.2014, PMCID: PMC4297861.
8. Kobayashi A, Mugford JW, Krautzberger AM, Naiman N, Liao J, McMahon AP. Identification of a multipotent self-renewing stromal progenitor population during mammalian kidney organogenesis. *Stem Cell Reports*. Oct 14 2014;3(4):650-662. doi:10.1016/j.stemcr.2014.08.008, PMCID: PMC4223698.
9. Little MH, Brennan J, Georgas K, Davies JA, Davidson DR, Baldock RA, Beverdam A, Bertram JF, Capel B, Chiu HS, Clements D, Cullen-McEwen L, Fleming J, Gilbert T, Herzlinger D, Houghton D, Kaufman MH, Kleymenova E, Koopman PA, Lewis AG, McMahon AP, Mendelsohn CL, Mitchell EK, Rumballe BA, Sweeney DE, Valerius MT, Yamada G, Yang Y, Yu J. A high-resolution anatomical ontology of the developing murine genitourinary tract. *Gene Expr Patterns*. Jun 2007;7(6):680-699. doi:10.1016/j.modgep.2007.03.002, PMCID: PMC2117077.
10. England AR, Chaney CP, Das A, Patel M, Malewska A, Armendariz D, Hon GC, Strand DW, Drake KA, Carroll TJ. Identification and characterization of cellular heterogeneity within the developing renal interstitium. *Development*. Aug 14 2020;147(15)doi:10.1242/dev.190108, PMCID: PMC7438011.
11. Airik R, Bussen M, Singh MK, Petry M, Kispert A. Tbx18 regulates the development of the ureteral mesenchyme. *J Clin Invest*. Mar 2006;116(3):663-674. doi:10.1172/JCI26027, PMCID: PMC1386107.
12. Drake KA, Chaney CP, Das A, Roy P, Kwartler CS, Rakheja D, Carroll TJ. Stromal beta-catenin activation impacts nephron progenitor differentiation in the developing kidney and may contribute to Wilms tumor. *Development*. Jul 31 2020;147(21)doi:10.1242/dev.189597, PMCID: PMC7406317.
13. Fetting JL, Guay JA, Karolak MJ, Iozzo RV, Adams DC, Maridas DE, Brown AC, Oxburgh L. FOXD1 promotes nephron progenitor differentiation by repressing decorin in the embryonic kidney. *Development*. Jan 2014;141(1):17-27. doi:10.1242/dev.089078, PMCID: PMC3865747.
14. Levinson RS, Batourina E, Choi C, Vorontchikhina M, Kitajewski J, Mendelsohn CL. Foxd1-dependent signals control cellularity in the renal capsule, a structure required for normal renal development. *Development*. Feb 2005;132(3):529-539. doi:10.1242/dev.01604, PMID: 15634693.
15. Yallowitz AR, Hrycaj SM, Short KM, Smyth IM, Wellik DM. Hox10 genes function in kidney development in the differentiation and integration of the cortical stroma. *PLoS One*. 2011;6(8):e23410. doi:10.1371/journal.pone.0023410, PMCID: PMC3156768.

16. Quaggin SE, Vanden Heuvel GB, Igarashi P. Pod-1, a mesoderm-specific basic-helix-loop-helix protein expressed in mesenchymal and glomerular epithelial cells in the developing kidney. *Mech Dev*. Feb 1998;71(1-2):37-48. doi:10.1016/s0925-4773(97)00201-3, PMID: 9507058.
17. Robb L, Mifsud L, Hartley L, Biben C, Copeland NG, Gilbert DJ, Jenkins NA, Harvey RP. epicardin: A novel basic helix-loop-helix transcription factor gene expressed in epicardium, branchial arch myoblasts, and mesenchyme of developing lung, gut, kidney, and gonads. *Dev Dyn*. Sep 1998;213(1):105-113. doi:10.1002/(SICI)1097-0177(199809)213:1<105::AID-AJA10>3.0.CO;2-1, PMID: 9733105.
18. Lu J, Richardson JA, Olson EN. Capsulin: a novel bHLH transcription factor expressed in epicardial progenitors and mesenchyme of visceral organs. *Mech Dev*. Apr 1998;73(1):23-32. doi:10.1016/s0925-4773(98)00030-6, PMID: 9545521.
19. Hidai H, Bardales R, Goodwin R, Quertermous T, Quertermous EE. Cloning of capsulin, a basic helix-loop-helix factor expressed in progenitor cells of the pericardium and the coronary arteries. *Mech Dev*. Apr 1998;73(1):33-43. doi:10.1016/s0925-4773(98)00031-8, PMID: 9545526.
20. Nagao M, Lyu Q, Zhao Q, Wirka RC, Bagga J, Nguyen T, Cheng P, Kim JB, Pjanic M, Miano JM, Quertermous T. Coronary Disease-Associated Gene TCF21 Inhibits Smooth Muscle Cell Differentiation by Blocking the Myocardin-Serum Response Factor Pathway. *Circ Res*. Feb 14 2020;126(4):517-529. doi:10.1161/CIRCRESAHA.119.315968, PMCID: PMC7274203.
21. Wirka RC, Wagh D, Paik DT, Pjanic M, Nguyen T, Miller CL, Kundu R, Nagao M, Coller J, Koyano TK, Fong R, Woo YJ, Liu B, Montgomery SB, Wu JC, Zhu K, Chang R, Alamprese M, Tallquist MD, Kim JB, Quertermous T. Atheroprotective roles of smooth muscle cell phenotypic modulation and the TCF21 disease gene as revealed by single-cell analysis. *Nat Med*. Aug 2019;25(8):1280-1289. doi:10.1038/s41591-019-0512-5, PMCID: PMC7274198.
22. Finer G, Maezawa Y, Ide S, Onay T, Souma T, Scott R, Liang X, Zhao X, Gadhvi G, Winter DR, Quaggin SE, Hayashida T. Stromal Transcription Factor 21 Regulates Development of the Renal Stroma via Interaction with Wnt/beta-Catenin Signaling. *Kidney360*. Jul 28 2022;3(7):1228-1241. doi:10.34067/KID.0005572021, PMCID: PMC9337899.
23. Quaggin SE, Schwartz L, Cui S, Igarashi P, Deimling J, Post M, Rossant J. The basic-helix-loop-helix protein pod1 is critically important for kidney and lung organogenesis. *Development*. Dec 1999;126(24):5771-5783. PMID: 10572052.
24. Adam M, Potter AS, Potter SS. Psychrophilic proteases dramatically reduce single-cell RNA-seq artifacts: a molecular atlas of kidney development. *Development*. Oct 1 2017;144(19):3625-3632. doi:10.1242/dev.151142, PMCID: PMC5665481.
25. Combes AN, Phipson B, Lawlor KT, Dorison A, Patrick R, Zappia L, Harvey RP, Oshlack A, Little MH. Single cell analysis of the developing mouse kidney provides deeper insight into marker gene expression and ligand-receptor crosstalk. *Development*. Jun 12 2019;146(12)doi:10.1242/dev.178673, PMID: 31118232.
26. Harding SD, Armit C, Armstrong J, Brennan J, Cheng Y, Haggarty B, Houghton D, Lloyd-MacGilp S, Pi X, Roochun Y, Sharghi M, Tindal C, McMahon AP, Gottesman B, Little MH, Georgas K, Aronow BJ, Potter SS, Brunskill EW, Southard-Smith EM, Mendelsohn C, Baldock RA, Davies JA, Davidson D. The GUDMAP database--an online resource for genitourinary research. *Development*. Jul 2011;138(13):2845-2853. doi:10.1242/dev.063594, PMCID: PMC3188593.
27. McMahon AP, Aronow BJ, Davidson DR, Davies JA, Gaido KW, Grimmond S, Lessard JL, Little MH, Potter SS, Wilder EL, Zhang P, project G. GUDMAP: the genitourinary developmental molecular anatomy project. *J Am Soc Nephrol*. Apr 2008;19(4):667-671. doi:10.1681/ASN.2007101078, PMID: 18287559.
28. Qiu X, Mao Q, Tang Y, Wang L, Chawla R, Pliner HA, Trapnell C. Reversed graph embedding resolves complex single-cell trajectories. *Nat Methods*. Oct 2017;14(10):979-982. doi:10.1038/nmeth.4402, PMCID: PMC5764547.
29. Trapnell C, Cacchiarelli D, Grimsby J, Pokharel P, Li S, Morse M, Lennon NJ, Livak KJ, Mikkelsen TS, Rinn JL. The dynamics and regulators of cell fate decisions are revealed by pseudotemporal ordering of single cells. *Nat Biotechnol*. Apr 2014;32(4):381-386. doi:10.1038/nbt.2859, PMCID: PMC4122333.
30. Mugford JW, Sipila P, McMahon JA, McMahon AP. Osr1 expression demarcates a multi-potent population of intermediate mesoderm that undergoes progressive restriction to an Osr1-dependent nephron progenitor compartment within the mammalian kidney. *Dev Biol*. Dec 1 2008;324(1):88-98. doi:10.1016/j.ydbio.2008.09.010, PMCID: PMC2642884.
31. Naiman N, Fujioka K, Fujino M, Valerius MT, Potter SS, McMahon AP, Kobayashi A. Repression of Interstitial Identity in Nephron Progenitor Cells by Pax2 Establishes the Nephron-Interstitium Boundary during Kidney Development. *Dev Cell*. May 22 2017;41(4):349-365 e343. doi:10.1016/j.devcel.2017.04.022, PMCID: PMC5532731.
32. Brunskill EW, Park JS, Chung E, Chen F, Magella B, Potter SS. Single cell dissection of early kidney development: multilineage priming. *Development*. Aug 2014;141(15):3093-3101. doi:10.1242/dev.110601, PMCID: PMC4197661.
33. Magella B, Adam M, Potter AS, Venkatasubramanian M, Chetal K, Hay SB, Salomonis N, Potter SS. Cross-platform single cell analysis of kidney development shows stromal cells express Gdnf. *Dev Biol*. Feb 1 2018;434(1):36-47. doi:10.1016/j.ydbio.2017.11.006, PMCID: PMC5930237.
34. Maezawa Y, Binnie M, Li C, Thorner P, Hui CC, Alman B, Taketo MM, Quaggin SE. A new Cre driver mouse line, Tcf21/Pod1-Cre, targets metanephric mesenchyme. *PLoS One*. 2012;7(7):e40547. doi:10.1371/journal.pone.0040547, PMCID: PMC3391250.
35. Bohnenpoll T, Bettenhausen E, Weiss AC, Foik AB, Trowe MO, Blank P, Airik R, Kispert A. Tbx18 expression demarcates multipotent precursor populations in the developing urogenital system but is exclusively required within the ureteric mesenchymal lineage to suppress a renal stromal fate. *Dev Biol*. Aug 1 2013;380(1):25-36. doi:10.1016/j.ydbio.2013.04.036, PMID: 23685333.
36. Funato N, Ohyama K, Kuroda T, Nakamura M. Basic helix-loop-helix transcription factor epicardin/capsulin/Pod-1 suppresses differentiation by negative regulation of transcription. *J Biol Chem*. Feb 28 2003;278(9):7486-7493. doi:10.1074/jbc.M212248200, PMID: 12493738.
37. Kanisicak O, Khalil H, Ivey MJ, Karch J, Maliken BD, Correll RN, Brody MJ, SC JL, Aronow BJ, Tallquist MD, Molkentin JD. Genetic lineage tracing defines myofibroblast origin and function in the injured heart. *Nat Commun*. Jul 22 2016;7:12260. doi:10.1038/ncomms12260, PMCID: PMC5512625.

Fig 1

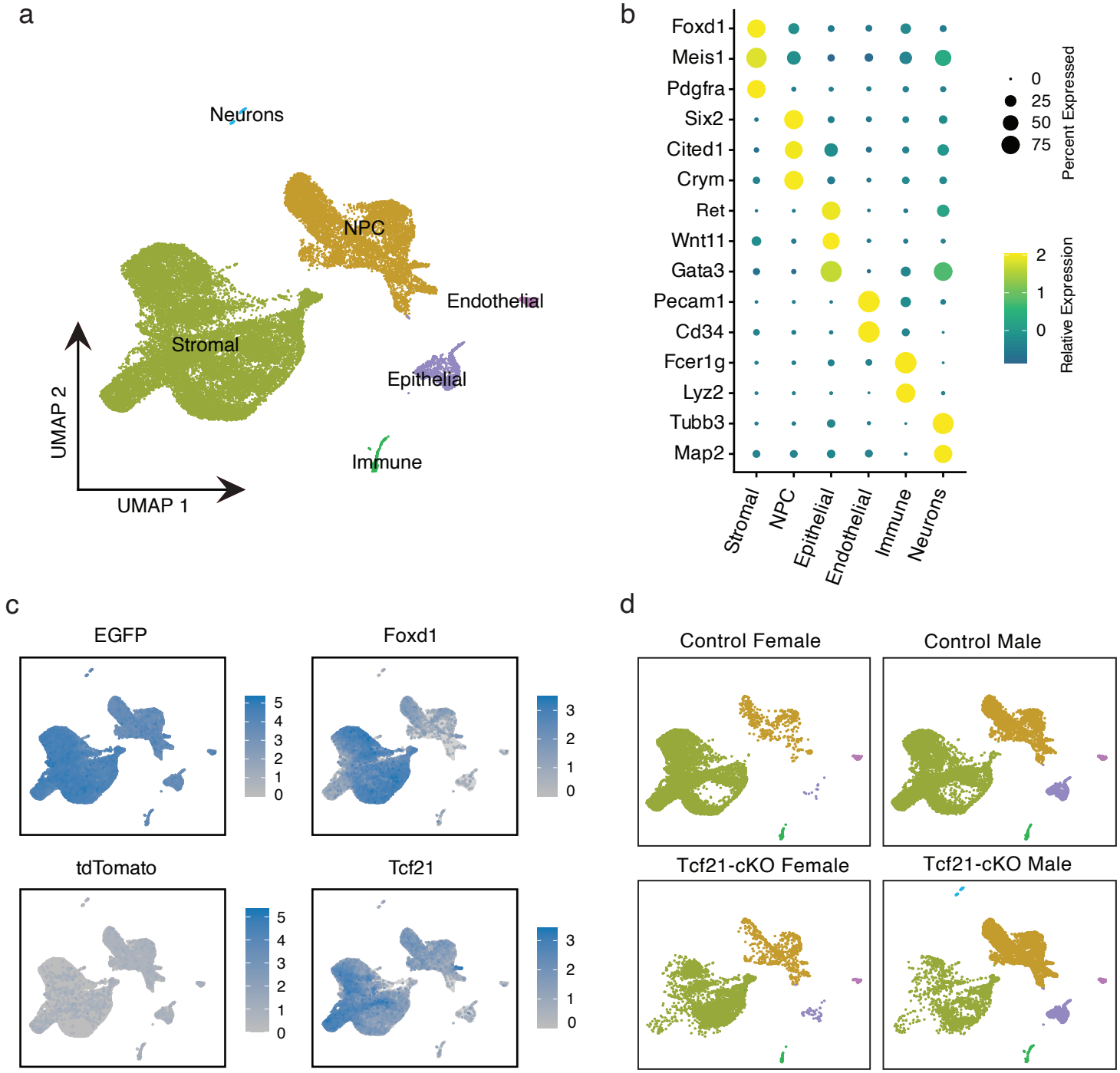
a
Neurons
NPC
Endothelial
Stromal
Epithelial
Immune
UMAP 2
UMAP 1
b
Foxd1
Meis1
Pdgfra
Six2
Cited1
Crym
Ret
Wnt11
Gata3
Pecam1
Cd34
Fcer1g
Lyz2
Tubb3
Map2
Stromal
NPC
Epithelial
Endothelial
Immune
Neurons
0
25
50
75
Percent Expressed
2
1
0
Relative Expression
c
EGFP
Foxd1
tdTomato
Tcf21
5
4
3
2
1
0
d
Control Female
Control Male
Tcf21-cKO Female
Tcf21-cKO Male

Fig 2

a

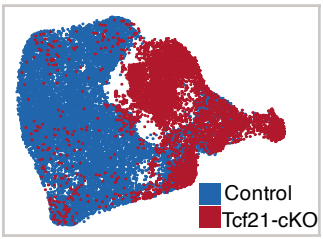
Control
Tcf21-cKO

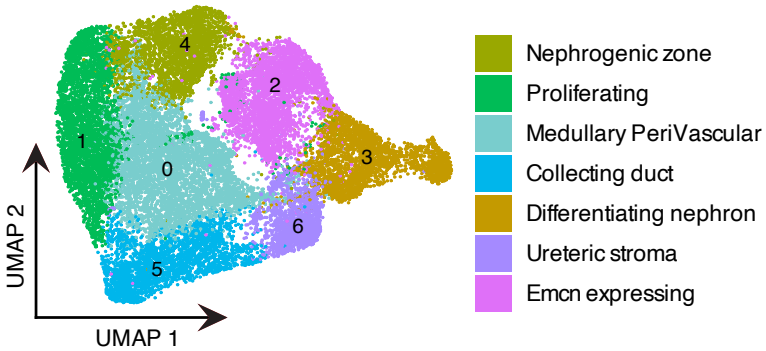
UMAP 2
UMAP 1
0
1
2
3
4
5
6
Nephrogenic zone
Proliferating
Medullary PeriVascular
Collecting duct
Differentiating nephron
Ureteric stroma
Emcn expressing

b

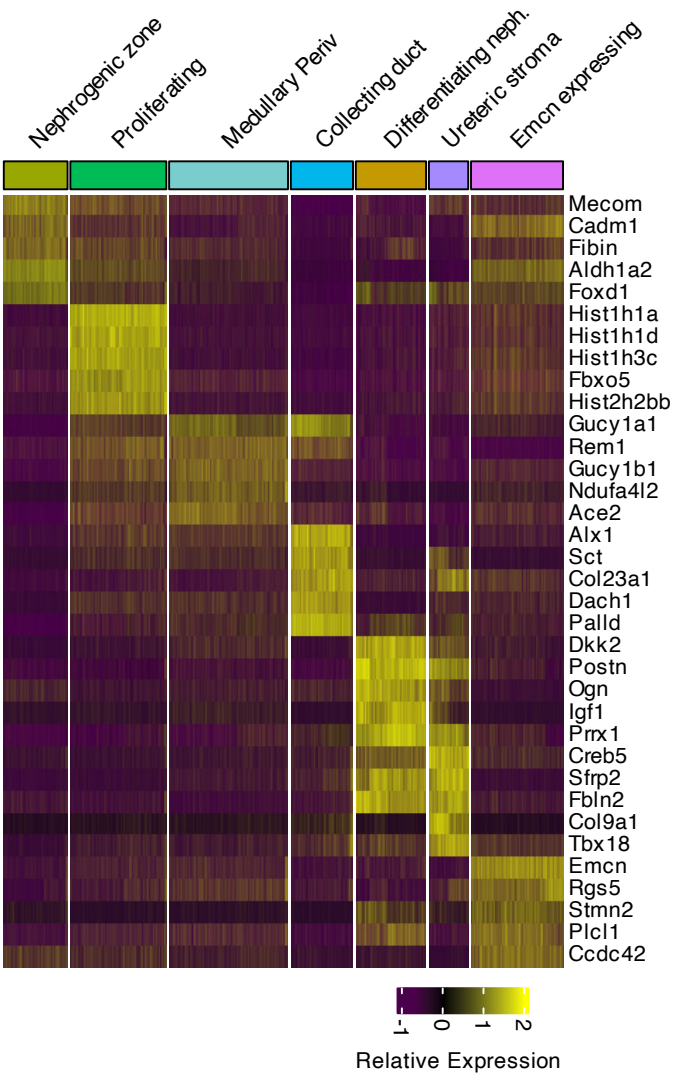
Nephrogenic zone
Proliferating
Medullary Periv
Collecting duct
Differentiating neph.
Ureteric stroma
Emcn expressing
Mecom
Cadm1
Fibin
Aldh1a2
Foxd1
Hist1h1a
Hist1h1d
Hist1h3c
Fbxo5
Hist2h2bb
Gucy1a1
Rem1
Gucy1b1
Ndufa4l2
Ace2
Alx1
Sct
Col23a1
Dach1
Palld
Dkk2
Postn
Ogn
Igf1
Prrx1
Creb5
Sfrp2
Fbln2
Col9a1
Tbx18
Emcn
Rgs5
Stmn2
Plcl1
Ccdc42
-1
0
1
2
Relative Expression

c

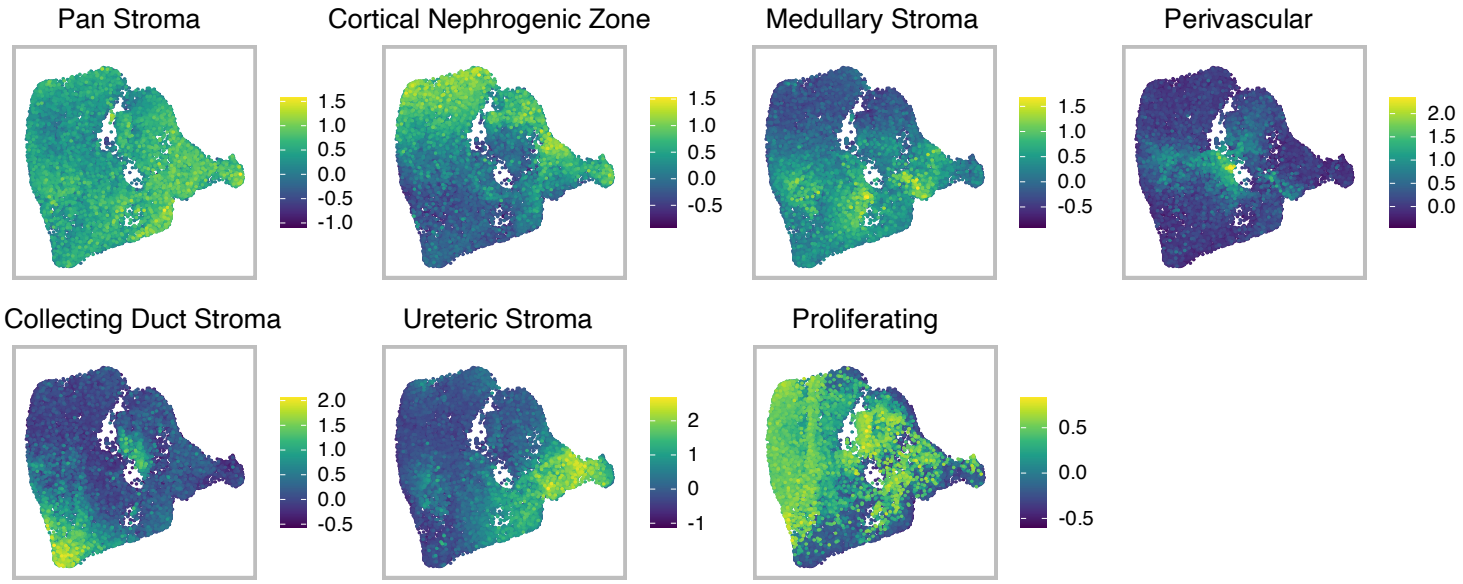
Pan Stroma
1.5
1.0
0.5
0.0
-0.5
-1.0
Cortical Nephrogenic Zone
1.5
1.0
0.5
0.0
-0.5
Medullary Stroma
1.5
1.0
0.5
0.0
-0.5
Perivascular
2.0
1.5
1.0
0.5
0.0
Collecting Duct Stroma
2.0
1.5
1.0
0.5
0.0
-0.5
Ureteric Stroma
2
1
0
-1
Proliferating
0.5
0.0
-0.5

Fig 3

a

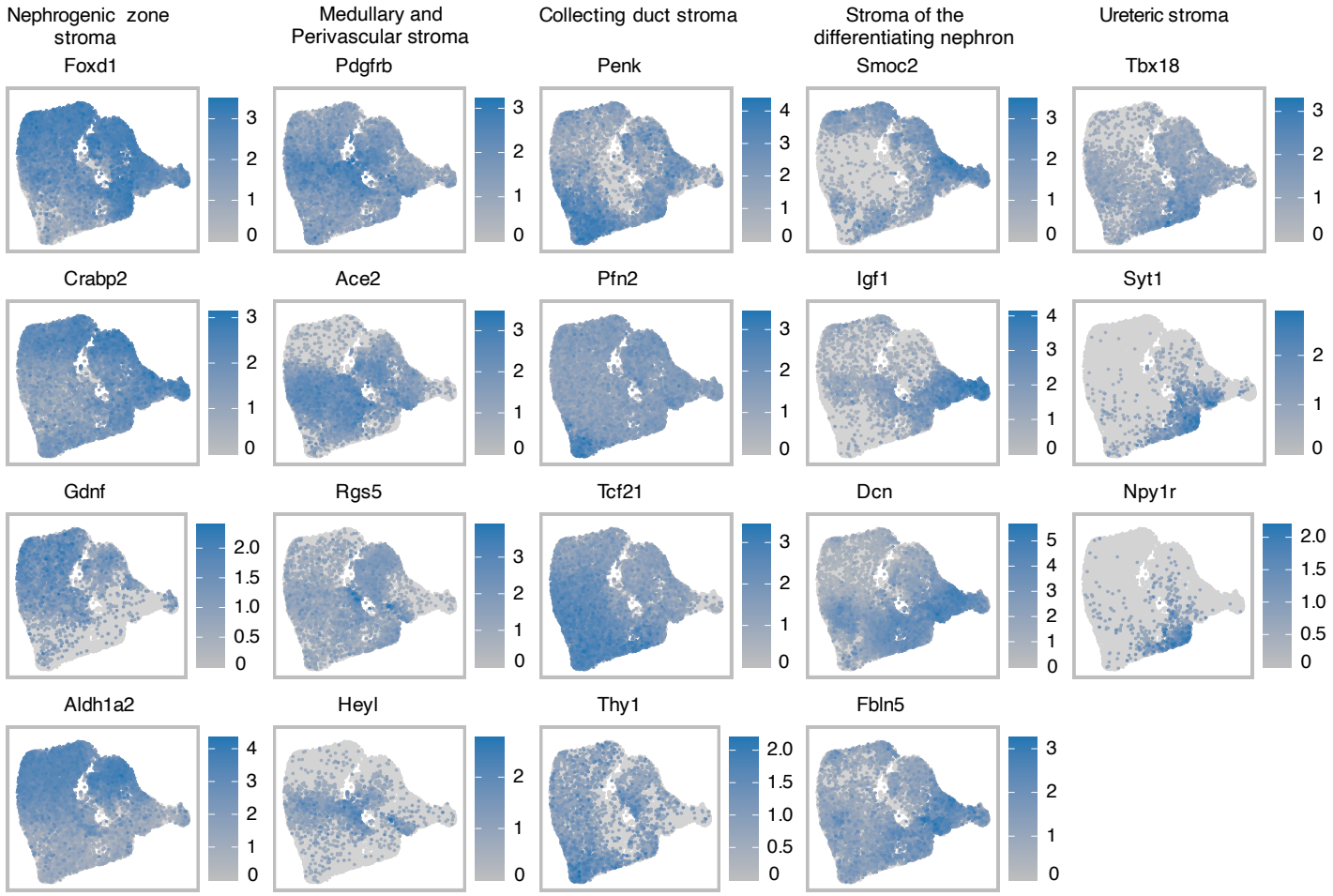
Nephrogenic zone stroma
Medullary and Perivascular stroma
Collecting duct stroma
Stroma of the differentiating nephron
Ureteric stroma
Foxd1
Pdgfrb
Penk
Smoc2
Tbx18
Crabp2
Ace2
Pfn2
Igf1
Syt1
Gdnf
Rgs5
Tcf21
Dcn
Npy1r
Aldh1a2
Heyl
Thy1
Fbln5

b

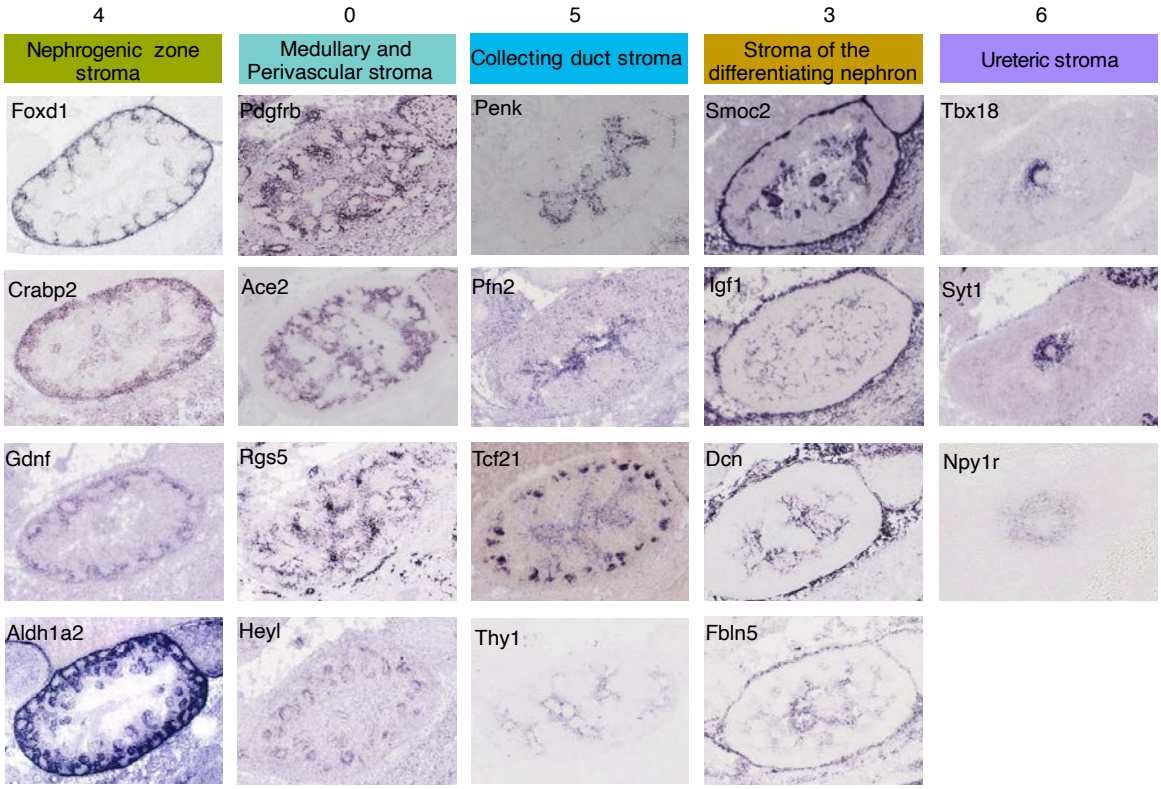
4
Nephrogenic zone stroma
0
Medullary and Perivascular stroma
5
Collecting duct stroma
3
Stroma of the differentiating nephron
6
Ureteric stroma
Foxd1
Pdgfrb
Penk
Smoc2
Tbx18
Crabp2
Ace2
Pfn2
Igf1
Syt1
Gdnf
Rgs5
Tcf21
Dcn
Npy1r
Aldh1a2
Heyl
Thy1
Fbln5

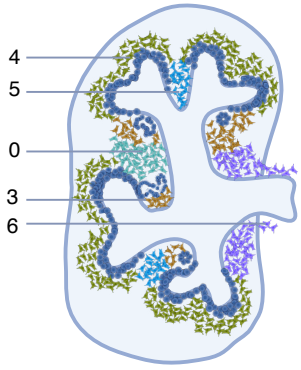
4
5
0
3
6

Fig 4

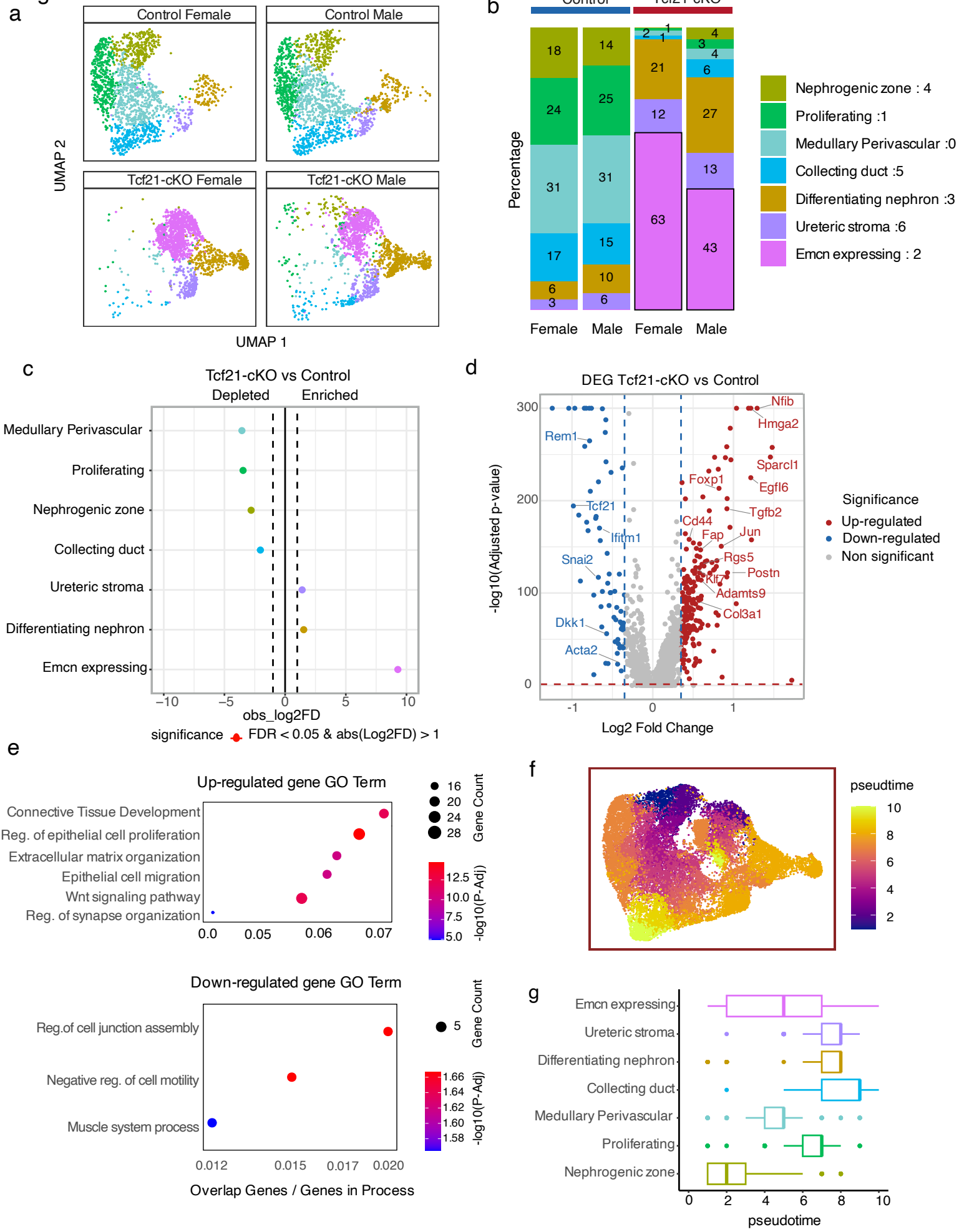
a
Control Female
Control Male
Tcf21-cKO Female
Tcf21-cKO Male
UMAP 2
UMAP 1
b
Control
Tcf21-cKO
Percentage
Female
Male
Female
Male
Nephrogenic zone : 4
Proliferating :1
Medullary Perivascular :0
Collecting duct :5
Differentiating nephron :3
Ureteric stroma :6
Emcn expressing : 2
c
Tcf21-cKO vs Control
Depleted
Enriched
Medullary Perivascular
Proliferating
Nephrogenic zone
Collecting duct
Ureteric stroma
Differentiating nephron
Emcn expressing
obs_log2FD
significance
FDR < 0.05 & abs(Log2FD) > 1
d
DEG Tcf21-cKO vs Control
-log10(Adjusted p-value)
Log2 Fold Change
Nfib
Hmga2
Rem1
Sparcl1
Foxp1
Egfl6
Tcf21
Tgfb2
Cd44
Ifitm1
Fap
Jun
Snai2
Rgs5
Postn
Klf7
Adamts9
Col3a1
Dkk1
Acta2
Significance
Up-regulated
Down-regulated
Non significant
e
Up-regulated gene GO Term
Connective Tissue Development
Reg. of epithelial cell proliferation
Extracellular matrix organization
Epithelial cell migration
Wnt signaling pathway
Reg. of synapse organization
Gene Count
-log10(P-Adj)
Down-regulated gene GO Term
Reg.of cell junction assembly
Negative reg. of cell motility
Muscle system process
Overlap Genes / Genes in Process
f
pseudtime
g
Emcn expressing
Ureteric stroma
Differentiating nephron
Collecting duct
Medullary Perivascular
Proliferating
Nephrogenic zone
pseudotime

Fig 5

a

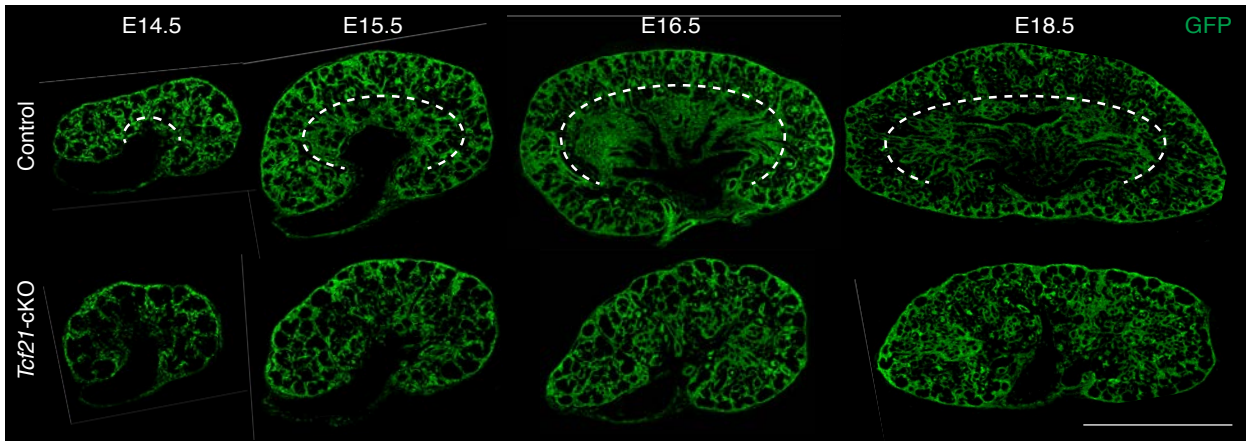
E14.5
E15.5
E16.5
E18.5
GFP
Control
Tcf21-cKO

b

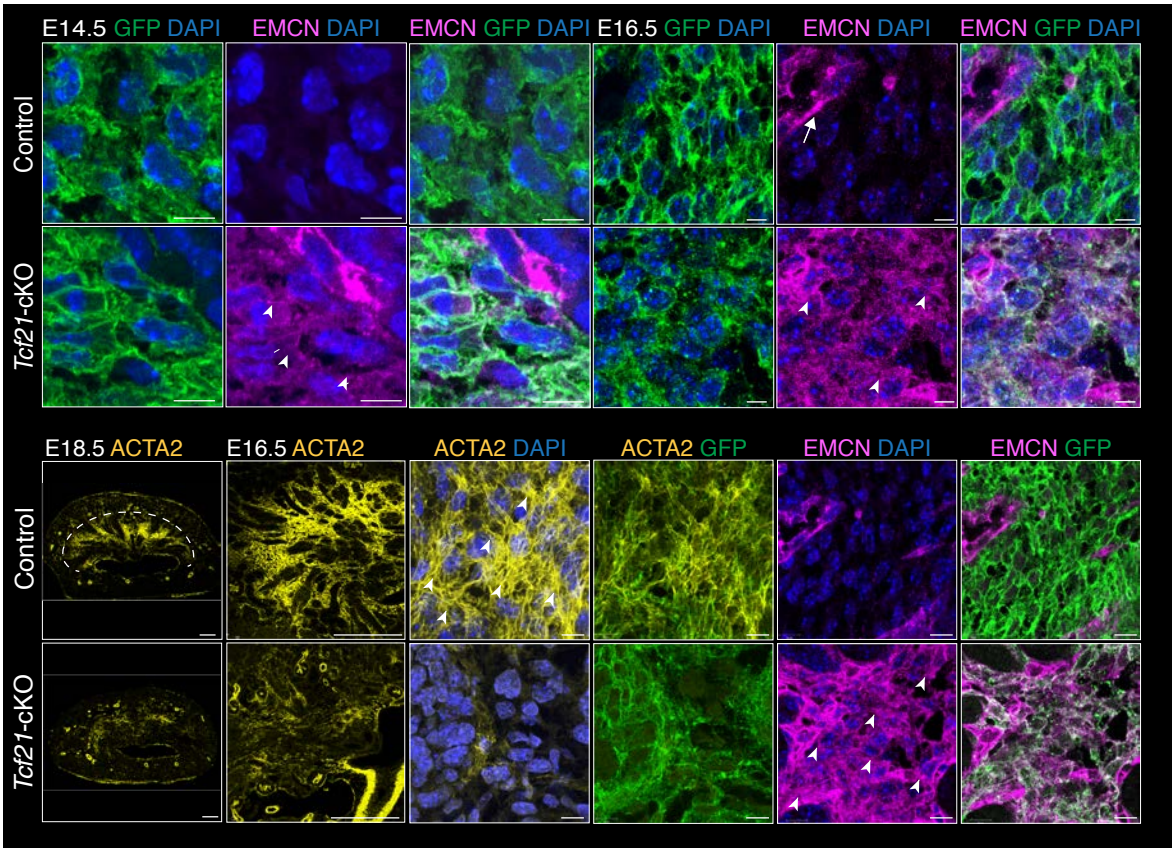
E14.5 GFP DAPI
EMCN DAPI
EMCN GFP DAPI
E16.5 GFP DAPI
EMCN DAPI
EMCN GFP DAPI
Control
Tcf21-cKO

c

E18.5 ACTA2
E16.5 ACTA2
ACTA2 DAPI
ACTA2 GFP
EMCN DAPI
EMCN GFP
Control
Tcf21-cKO

d

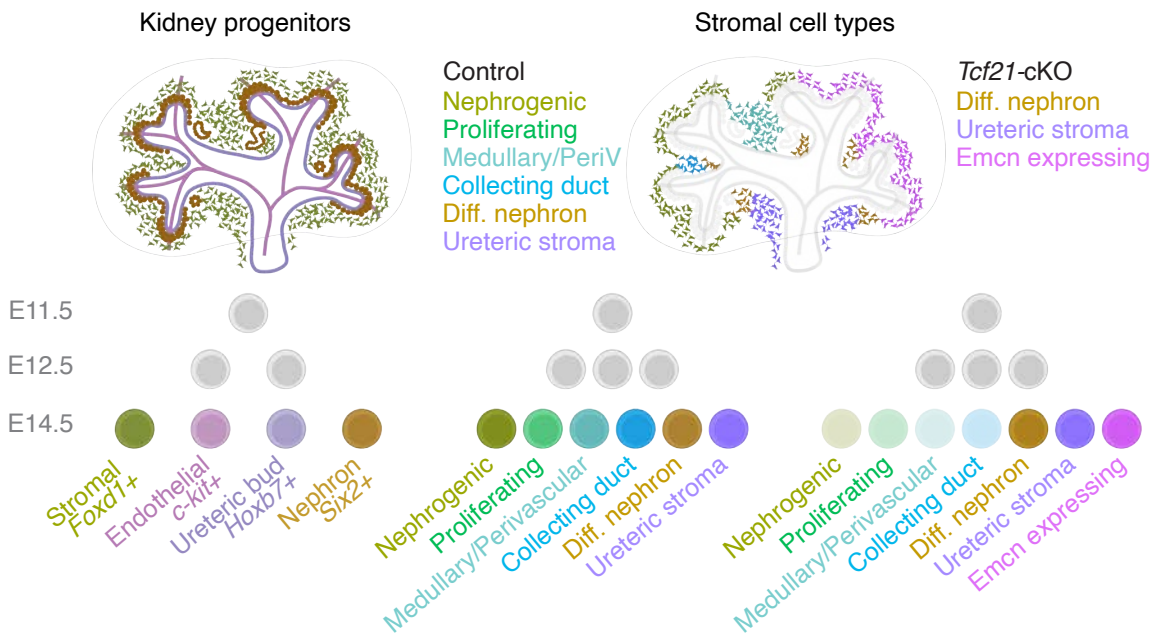
Kidney progenitors
Stromal cell types
Control
Nephrogenic
Proliferating
Medullary/PeriV
Collecting duct
Diff. nephron
Ureteric stroma
Tcf21-cKO
Diff. nephron
Ureteric stroma
Emcn expressing
E11.5
E12.5
E14.5
Stromal Foxd1+
Endothelial c-kit+
Ureteric bud Hoxb7+
Nephron Six2+
Nephrogenic
Proliferating
Medullary/Perivascular
Collecting duct
Diff. nephron
Ureteric stroma
Nephrogenic
Proliferating
Medullary/Perivascular
Collecting duct
Diff. nephron
Ureteric stroma
Emcn expressing

Suppl Fig 1

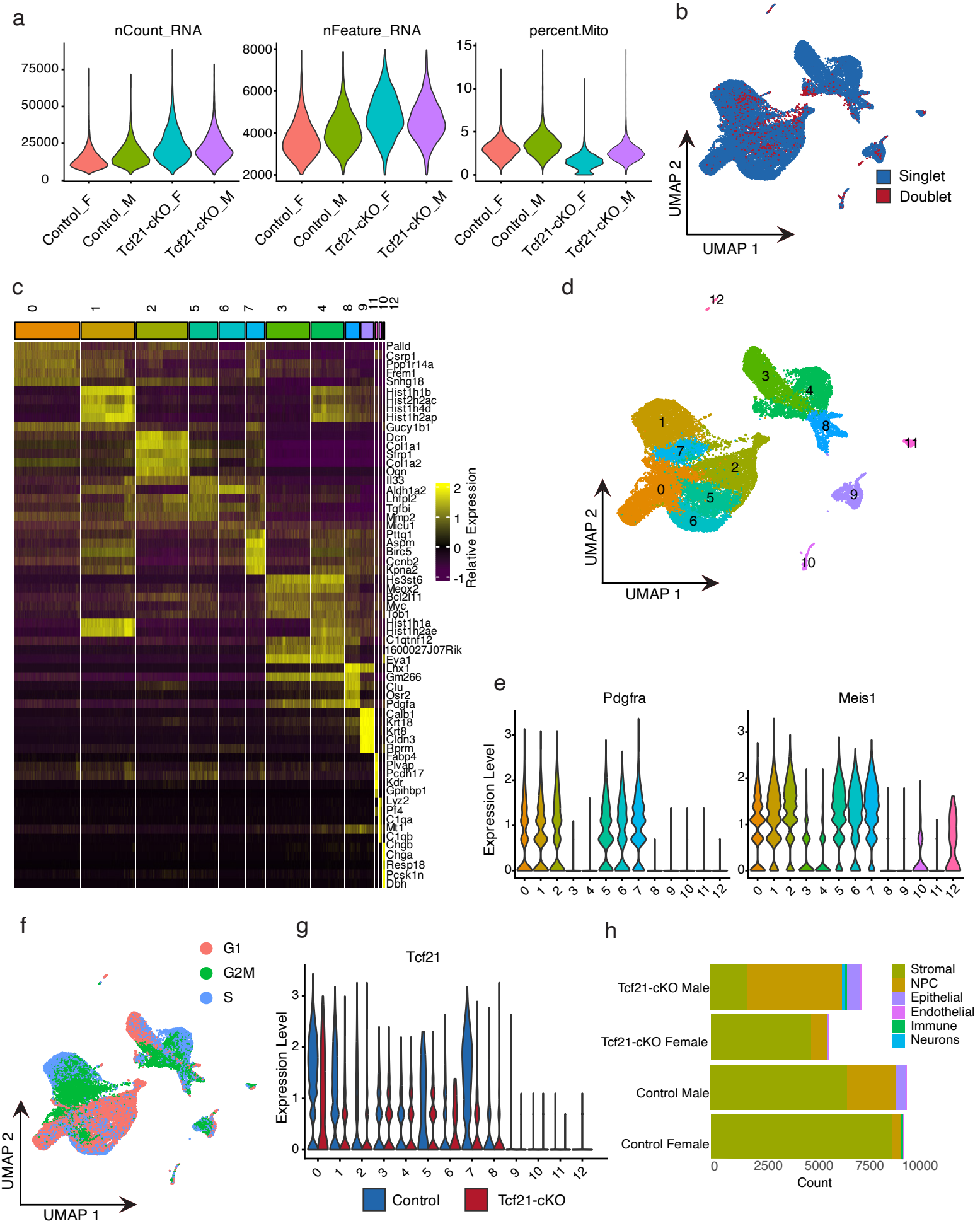
a
nCount_RNA
nFeature_RNA
percent.Mito
Control_F
Control_M
Tcf21-cKO_F
Tcf21-cKO_M
b
UMAP 2
UMAP 1
Singlet
Doublet
c
Relative Expression
d
UMAP 2
UMAP 1
e
Pdgfra
Meis1
Expression Level
f
G1
G2M
S
UMAP 2
UMAP 1
g
Tcf21
Expression Level
Control
Tcf21-cKO
h
Tcf21-cKO Male
Tcf21-cKO Female
Control Male
Control Female
Stromal
NPC
Epithelial
Endothelial
Immune
Neurons
Count

Suppl Fig 2

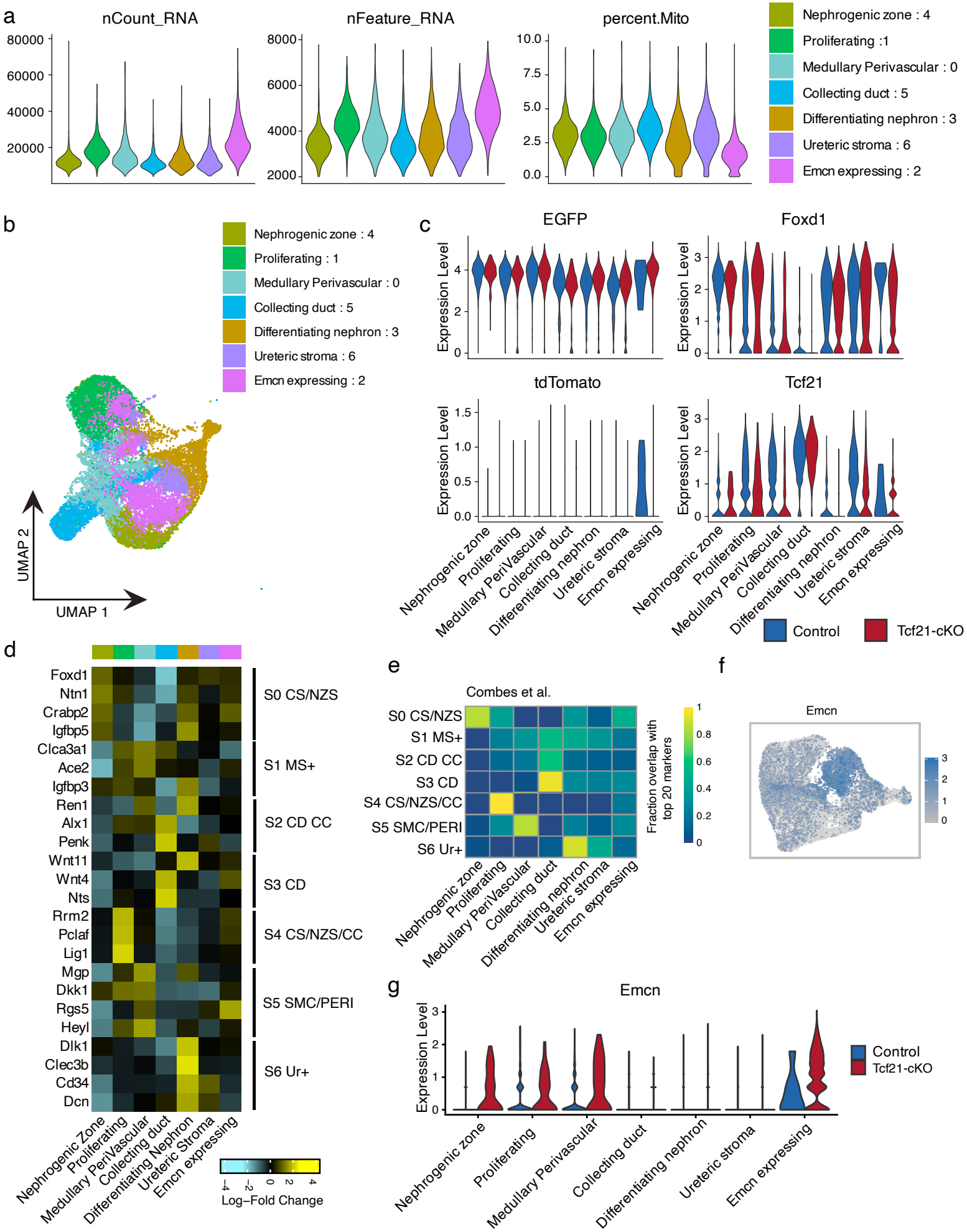
a
nCount_RNA
nFeature_RNA
percent.Mito
Nephrogenic zone : 4
Proliferating :1
Medullary Perivascular : 0
Collecting duct : 5
Differentiating nephron : 3
Ureteric stroma : 6
Emcn expressing : 2
b
UMAP 2
UMAP 1
c
EGFP
Foxd1
tdTomato
Tcf21
Expression Level
Nephrogenic zone
Proliferating
Medullary PeriVascular
Collecting duct
Differentiating nephron
Ureteric stroma
Emcn expressing
Control
Tcf21-cKO
d
Foxd1
Ntn1
Crabp2
Igfbp5
Clca3a1
Ace2
Igfbp3
Ren1
Alx1
Penk
Wnt11
Wnt4
Nts
Rrm2
Pclaf
Lig1
Mgp
Dkk1
Rgs5
Heyl
Dlk1
Clec3b
Cd34
Dcn
S0 CS/NZS
S1 MS+
S2 CD CC
S3 CD
S4 CS/NZS/CC
S5 SMC/PERI
S6 Ur+
Nephrogenic Zone
Proliferating
Medullary PeriVascular
Collecting duct
Differentiating Nephron
Ureteric Stroma
Emcn expressing
Log−Fold Change
e
Combes et al.
S0 CS/NZS
S1 MS+
S2 CD CC
S3 CD
S4 CS/NZS/CC
S5 SMC/PERI
S6 Ur+
Fraction overlap with top 20 markers
f
Emcn
g
Emcn
Expression Level
Control
Tcf21-cKO

Suppl Fig 3

Cell Type	Marker	Reference
Pan-stroma	Pdgfra	1,2
	Col3a1	1,2
	Meis1	1,2
	Cited1	1,2
	Meis2	1,2,3
Cortical/Nephrogenic Zone	Ntn1	1,3
	Igfbp5	1,3
	Foxd1	1,2,3
	Plag1	3
	Aldh1a2	3
	Gdnf	3
	Smoc2	2
	Fibin	2
Medullary Stroma	Clca3a1	1,3
	Ace2	1,4
	Igfbp3	1,3
	Acta2	1,2,4,5
	Col4a1	3
	Zeb2	3
	Col1a1	3
	Tgfb1i1	2
Perivascular	Akr1b7	2
	Ren1	2
	Rgs5	1,3
	Heyl	1,3
	Pdgfrb	1,3,5
	Igf	1,2
	Mef2c	3,5
	Angpt2	1,3
Collecting Duct Stroma	Wnt4	1,3
	Penk	1,2,3
	Alx1	1,3
	Sema3c	1,4
	Lef1	2,5
	Nkd1	3
	Col15a1	1,3
Ureteric Stroma	Dcn	1,3
	Sparc	1
	Igf1	2,3
	Tbx18	2,3,4,6
	Sfrp2	3
	Dlk1	1,2
	Igbp6	3

Reference:

1. Combes AN, Phipson B, Lawlor KT, Dorison A, Patrick R, Zappia L, Harvey RP, Oshlack A, and Little MH. Development 146: 2019.
2. England AR, Chaney CP, Das A, Patel M, Malewska A, Armendariz D, Hon GC, Strand DW, Drake KA, and Carroll TJ. Development 147: 2020.
3. Allen Developing Mouse Brain Atlas
4. McMahon AP, Aronow BJ, Davidson DR, Davies JA, Gaido KW, Grimmond S, Lessard JL, Little MH, Potter SS, Wilder EL, Zhang P, and project GUDMAP. J Am Soc Nephrol 19: 2008.
5. Finer G, Maezawa Y, Ide S, Onay T, Souma T, Scott R, Liang X, Zhao X, Gadhvi G, Winter DR, Quaggin SE, and Hayashida T. Kidney360 3: 2022.
6. Bohnenpoll T, Bettenhausen E, Weiss AC, Foik AB, Trowe MO, Blank P, Airik R, and Kispert A. Dev Biol 380: 2013.

Suppl Fig 4

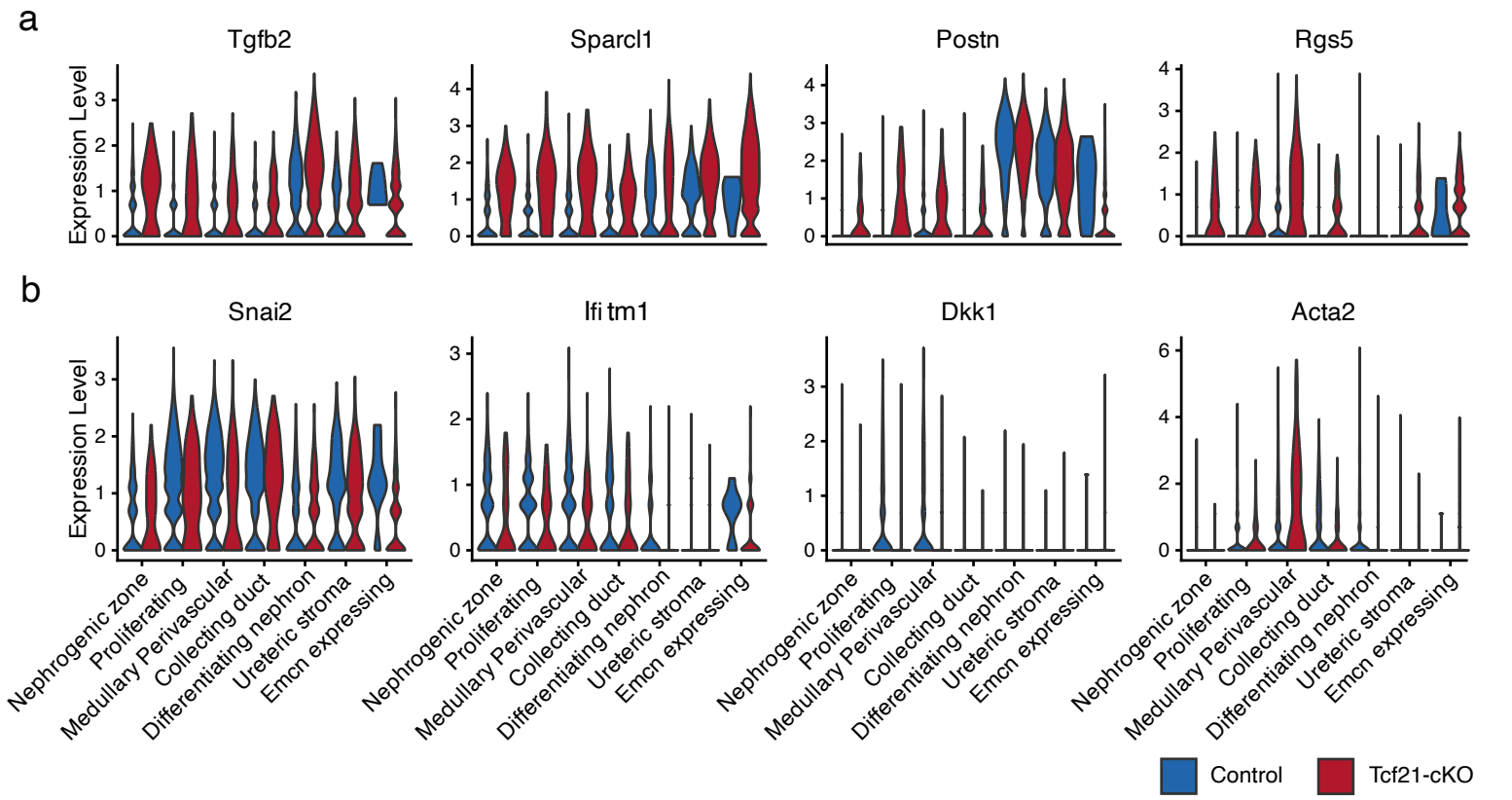
a
Tgfb2
Sparcl1
Postn
Rgs5
Expression Level
b
Snai2
Ifi tm1
Dkk1
Acta2
Expression Level
Nephrogenic zone
Proliferating
Medullary Perivascular
Collecting duct
Differentiating nephron
Ureteric stroma
Emcn expressing
Control
Tcf21-cKO

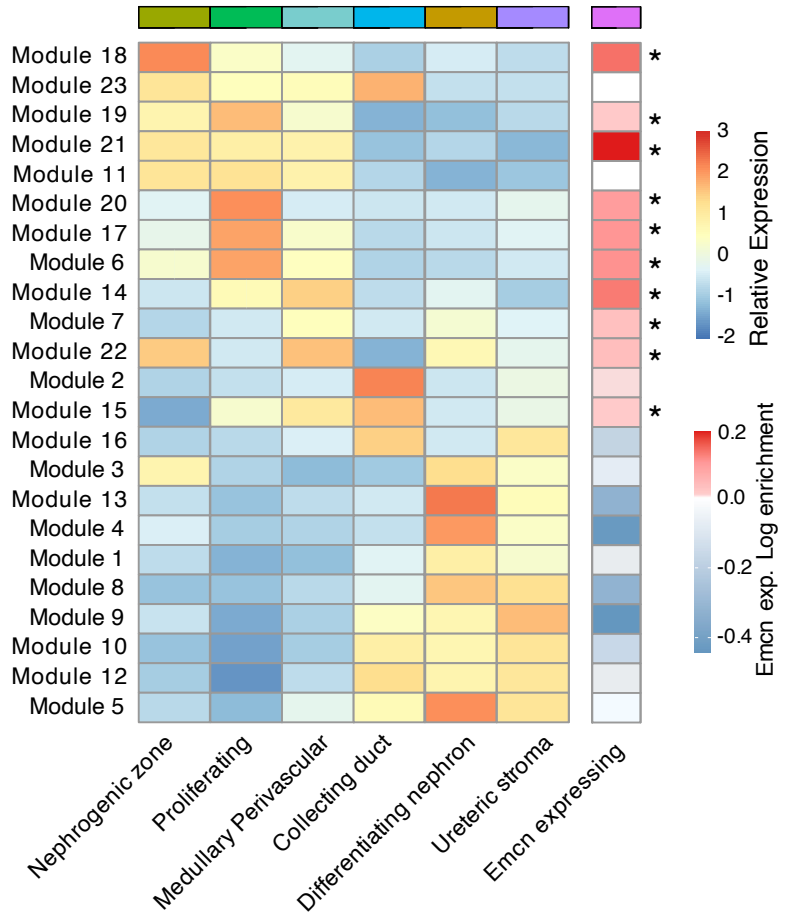
c
Module 18
Module 23
Module 19
Module 21
Module 11
Module 20
Module 17
Module 6
Module 14
Module 7
Module 22
Module 2
Module 15
Module 16
Module 3
Module 13
Module 4
Module 1
Module 8
Module 9
Module 10
Module 12
Module 5
Relative Expression
Emcn exp. Log enrichment
Nephrogenic zone
Proliferating
Medullary Perivascular
Collecting duct
Differentiating nephron
Ureteric stroma
Emcn expressing

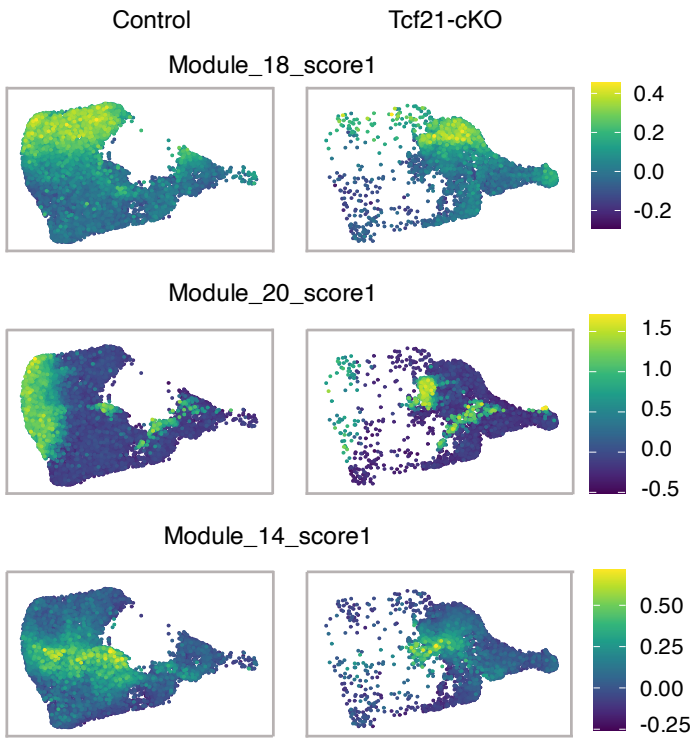
d
Control
Tcf21-cKO
Module_18_score1
Module_20_score1
Module_14_score1